Pablo Alvarez Santos

may.-21

High-power density electric motors for regional aircraft propulsion

High-power density electric motors for regional aircraft propulsion

PROYECTO

presentado para optar

al Título de Máster en Ingeniería Industrial por

Pablo Alvarez Santos

bajo la supervisión de

Marco Satrústegui De Legarra

Donostia-San Sebastián, mayo de 2021

tecnun
Universidad de Navarra

Pablo Alvarez Santos: *High-power density electric motors for regional aircraft propulsion* in *CEIT, San Sebastian, Spain.* May 2021.

Universidad de Navarra Escuela Superior de Ingenieros

Nafarroako Unibertsitatea Ingeniarien Goi Mailako Eskola

Proyecto Fin de Máster

INGENIERIA INDUSTRIAL

High-power density electric motors for regional aircraft propulsion

Pablo Alvarez Santos

San Sebastián, mayo de 2021

tecnun

CAMPUS TECNOLÓGICO DE LA UNIVERSIDAD DE NAVARRA. NAFARROAKO UNIBERTSITATEKO CAMPUS TEKNOLOGIKOA

Paseo de Manuel Lardizábal 13. 20018 Donostia-San Sebastián. Tel.: 943 219 877 Fax: 943 311 442 www.tecnun.es informacion@tecnun.es

Abstract

This Master's thesis project aims, firstly, to evaluate the current state of the art in aeronautical propulsion technology using electric machines. Once the state of the art has been studied, a tool for the design and calculation of electric motors with superconducting windings is developed in order to present a pre-design that meets the established objectives.

The analysis carried out on the state of the art will provide information on the design guidelines that have been taken in recent years, as well as the different projects and studies that are planned for the medium-term future. Thanks to this framework, geometric and performance requirements of the motor are defined together with the objectives to be met.

In order to achieve this goal, a superconducting motor design module is implemented in Matlab and FEMM, which helps to develop the selected motor efficiently, rapidly and accurately. The IPED electric machine design tool is described, and the different stages in the calculation of the motor are explained in detail.

Finally, the conclusions drawn from the different chapters are summarised, which will serve as a guideline for the continuation of the HIVOMOT project, in which this Master's thesis is framed.

Keywords: electric motor, aeronautics, high-temperature superconductors, high power, high voltage.

Resumen

El presente proyecto de fin de Máster trata, en primer lugar, de realizar una evaluación sobre el estado actual de la tecnología de la propulsión aeronáutica mediante máquinas eléctricas. Una vez estudiado el estado del arte, se desarrolla una herramienta de diseño y cálculo de motores eléctricos con devanados superconductores con el fin de presentar un prediseño que cumpla con los objetivos establecidos.

El análisis realizado sobre el estado de la tecnología permitirá conocer las líneas de diseño que se han tomado en los últimos años, así como los diferentes proyectos y estudios que están previstos en un futuro a medio plazo. Gracias a este marco de trabajo se definen unos requerimientos geométricos y de prestaciones del motor junto con unos objetivos a cumplir.

Para poder alcanzar esta meta se implementa un módulo de diseño de motores superconductores en Matlab y FEMM que ayuda a desarrollar el motor seleccionado de forma eficaz, rápida y precisa. Se describe la herramienta de diseño de máquinas eléctricas IPED, y se explica de forma detallada las diferentes etapas en el cálculo del motor.

Por último, se resumen las conclusiones extrapoladas en los diferentes capítulos y que servirán como pauta de cara a la continuación del proyecto HIVOMOT, en el que se encuentra enmarcado este proyecto de Fin de Máster.

Palabras clave: motor eléctrico, aeronáutica, superconductores de alta temperatura, alta potencia, alto voltaje.

Acknowledgements

Thank you,

to my tutor, Marco Satrústegui De Legarra, for his constant monitoring, attention, willingness and disposition at all times during the development of this project and to the whole Electric Vehicle group at CEIT;

to the University of Navarra and the School of Engineering of Tecnun for the academic and personal training provided over the last six years, which is now concluded with this Final Degree Project. I would like to thank all the teachers for their involvement with each student and especially to Iñigo Gutiérrez García for advising me in this training cycle;

to my family, Luis, Begoña, Laura and Maddi for being the most solid support during these six years and, above all, during the last twenty-four. Special thanks to you because without your help, education and unconditional support I would not be anywhere near where I am today;

thank you.

List of Contents

Page

Abstract V

Resumen VII

Acknowledgements IX

List of Contents XI

List of Figures XIII

List of Tables XV

List of Acronyms XVII

Introduction 1

1.1. Background 1
1.2. Framework 2
1.3. Aim of the Project 2

State of the Art in HTS Aircraft Propulsion 5

2.1. Aircraft Electric Propulsion 5
2.1.1. Electric Propulsion Configurations 6
2.1.2. Distributed Propulsion 7
2.2. History of the Electric Aircraft 9
2.2.1. Earliest Designs. Gliders 9
2.2.2. More Powerful Electric Aircrafts. Milestones and larger Companies 10

2.2.3. Latest Flyable Designs. Most powerful EPAC 11
2.3. Electric Aircraft Concepts and Studies 14
2.3.1. Short-term Flyable Aircrafts 14
2.3.2. Larger and MW-class Concepts. BLI and HTS Technologies 15
2.3.2.1. Boundary Layer Ingestion (BLI) 15
2.3.2.2. Superconductivity 16
2.4. High Voltage Electrical Systems at High Altitude 19
2.5. High Temperature Superconductors (HTS) 21
2.5.1. Electrical Energy Distribution 21
2.5.2. Electrical Machines 22
2.5.3. HTS Materials 23
2.6. Conclusions 26
2.6.1. Electromagnetic requirements 26
2.6.1.1. Output power 26
2.6.1.2. Rotational speed 27
2.6.1.3. Power density and efficiency 27
2.6.1.4. Power converter requirements 27
2.6.1.5. Summary 28
2.6.2. Volume requirements 29
2.6.2.1. Propulsion in regional aircrafts 29
2.6.2.2. Summary 30
2.6.3. HTS motor topology requirements 30
2.6.4. Cryogenic cooling system requirements 31

HTS Electric Motor Design Module 33

3.1. IPED® 33
3.2. HTS Module 34
3.2.1. Structure of the HTS Module 35
3.2.1.1. Input Data 35
3.2.1.2. Dependant Variables 36
3.2.1.3. Machine drawing 37
3.2.1.4. FEMM® Configuration 39
3.2.1.5. Calculation 40
3.2.1.6. Machine results 45
3.2.2. Conclusions 49

Predesign 51

4.1. First Proposed Design 51
4.2. Optimization of the Stator 53

Conclusions and future work 57

5.1. Conclusions 57
5.2. Future work 58

Bibliography 59

List of Figures

Figure 1. Electric propulsion principal configurations. 6
Figure 2. Basic configuration of a 4-motor distributed propulsion. 8
Figure 3. Lange Antares 20E (Lange Aviation image). 9
Figure 4. Timeline of Airbus' electric propelled projects (Airbus image). 10
Figure 5. Temporary evolution of electric propulsion power (data from **Table 1**). 12
Figure 6. Temporary evolution of maximum take-off weight (data from **Table 1**). 13
Figure 7. NASA's X-57 'Maxwell' airplane (NASA image). 14
Figure 8. Illustration of the wasted kinetic energy comparison between a conventional aircraft (top) and an aircraft with BLI (bottom) [85]. 15
Figure 9. BLI at the tail of the Ampaire Tailwind (Ampaire image). 16
Figure 10. Ongoing studies and projects of electric propulsion (data from **Table 2**). 18
Figure 11. Paschen Curve for the case of two parallel plates [86]. 19
Figure 12. Scheme of the study of partial discharge on conductors by Hayakawa *et al.* [55]. 21
Figure 13. 10 MW generator field coil designed by Sarmiento *et al.* [57]. 22
Figure 14. Radial view of 1-MW propulsion motor designed by Zhang *et al* [59]. 23
Figure 15. MgB_2 wires for superconducting cable demonstrator. 24
Figure 16. Timeline of the discovery of different superconducting materials (data from **Table 3**). 25
Figure 17. Main features of the E-Fan-X test aircraft obtained from the call. 26
Figure 18. Nacelle cross section with global dimensions in a ducted fan [81]. 29
Figure 19. Visualized nacelle geometry for different nacelle diameters [82]. 30
Figure 20. Frontal section of the proposed HTS motor. 34
Figure 21. Detail of the stator (left) and rotor (right) winding. 35

Figure 22. HTS Module structure. 35
Figure 23. Relation of the dependant variables of the model. 36
Figure 24. Frontal section (up), transversal section (centre) and stator slot (bottom) of the machine 38
Figure 25. Detail of the rotor pole and winding (up) and the rotor end winding (bottom). 39
Figure 26. FEMM calculation structure. 42
Figure 27. Geometric FEMM definition of the stator (up, left), the rotor (up, right) and the machine mesh (bottom). 43
Figure 28. Obtention of the operating point current. 44
Figure 29. Map colour of the flux density in the motor. 45
Figure 30. Different views of the motor on MotorCAD® and IPED® software. 47
Figure 31. Flux density results on MotorCAD® (up) and IPED® (down). 48
Figure 32. Different views of the motor on the IPED® software. 52
Figure 33. Flux density results on IPED®. 53
Figure 34. Different views of the optimized motor on IPED®. 54
Figure 35. Flux density results on IPED®. 56

List of Tables

Table 1 Summary of manned electric aircrafts [1]. 11
Table 2 Summary of electric aircraft concepts and studies [1]. 17
Table 3 Summary of superconducting materials. 25
Table 4 Electric motor concepts developed for aircraft applications. 27
Table 5 Main features of the power converter. 28
Table 6 Electromagnetic requirements. 28
Table 7 Main dimensions of the propulsion system in a regional aircraft. 30
Table 8 Preliminary motor topology. 31
Table 9 Preliminary motor topology. 31
Table 10 Summary of the motor power parameters (1st design). 49
Table 11 Summary of the requirements of the HIVOMOT project. 51
Table 12 Summary of the rotor parameters. 52
Table 13 Summary of the motor power parameters (1st design). 53
Table 14 Summary of the motor power parameters (2nd design). 55
Table 15 Mass breakdown of the motor (2nd design). 55

List of Acronyms

A/C	**A**ir**c**raft
AC	**A**lternating **C**urrent
BLI	**B**oundary **L**ayer **I**ngestion
DC	**D**irect **C**urrent
EMF	**E**lectro**m**agnetic **F**orce
EPAC	**E**lectric **P**ropelled **A**ir**c**raft
HTS	**H**igh **T**emperature **S**uperconductor
IM	**I**nduction **M**otor
LTS	**L**ow **T**emperature **S**uperconductor
MTPA	**M**aximum **T**orque **P**er **A**mpere
PMSM	**P**ermanent **M**agnet **S**ynchronous **M**achine
SC	**S**uper**c**onductor
SPSM	**S**alient **P**ole **S**ynchronous **M**achine

Chapter 1

Introduction

1.1. Background

The European Union is trying to reduce CO_2 emissions and fossil fuel consumption, and one of the biggest pollutants today is aviation. To tackle this problem, the implementation of electric motors in aircraft propulsion has been researched for years. However, the power densities required for these motors are far higher than the needed in other transport sectors (such as the railway or the automotive) as they substitute high power gas turbines. Therefore, it has not been developed an electric motor that fulfils the objectives.

The fundamental problem is weight. An aircraft has very specific load limitations depending on the power provided by the engines, requiring indeed high-power density electric motors. In addition, the current electric battery technology comes as another relevant issue in medium and big size airplanes where the required energy storage is increased. On the other hand, in the case of prototype or unmanned aircraft, these power density and energy storage levels are more feasible since the mass of these models is not very high [1], whereas for larger passenger aircrafts the power required ascends to MW-class range.

To date some remarkable work has been done in this area both with developed and flyable electric aircrafts and with studies and projects with a medium or long-term regard. Nevertheless, to develop

a regional electric aircraft disruptive technology such as High Temperature Superconductors or distributed propulsion is needed.

The primary objective of this project is to contribute to the development of the more electric aircraft. In particular, a pre-design of a MW-class HTS electric motor will be developed to fulfil the required aims defined on the work.

1.2. Framework

The content of this thesis is framed within the research activities on rotating electrical machines conducted by the research group of Electric Vehicle at *Ceit BRTA*, in San Sebastian, Spain.

Electrical machines have been investigated in this research group for more than 20 years, in which several projects and work related to the design, manufacturing, control, construction and simulation regarding different machine topologies have been conducted.

The present research work arises as a response to the European Commission call *Advanced High-Power Electrical Systems for High Altitude Operation (JTI-CS2-2020-CFP11-THT-12).* This call belongs to the *Horizon 2020 Framework Programme*, as part of the *H2020-JTI-CLEANSKY-2020-2021* programme part.

The official title of the project where this work framed is HIVOMOT (High power and Voltage operation for electric motors in aeronautics) and has been funded by the European Union (ID: H2020-EU.3.4.5.10.). For this Project a consortium formed by 4 companies has been formed, consisting of:

- Ceit BRTA [2].
- Suprasys SL [3].
- Antec Magnets SLU [4].
- Alconza Berango SL [5].

1.3. Aim of the Project

The aim of this project is to investigate solutions for the scientific and technical challenges regarding the use of high power and high voltage electric motors at high altitude conditions. Research into the implications of high voltage and altitude in the reliability and safety of actual systems and its

technical solutions, but also investigation into new HTS based electric drives for these conditions are proposed.

The main objective splits into the following technical objectives:

- Development of a state of the art about electric machines for electric aircraft propulsion regarding both the history of the electric aircraft and the concepts and studies expected for the following years. Also, high temperature superconductors are analysed and discussed in order to compare them and to choose the most suitable one for this specific project.
- Development of a superconducting electric motor calculation tool implemented in the IPED® software in order to obtain results for the proposed electric machine.
- Preliminary design and comparison of different HTS based electric machine topologies for aircraft applications at high voltage and high altitude in terms of power density, reliability and safety.

Chapter 2

State of the Art in HTS Aircraft Propulsion

In order to develop an electric motor for aircraft application with High Temperature Superconductors, a review about the current State of the Art is required. First of all, the most common electric propulsion configurations are listed. Then, both the history of the electric aircraft and future electric aircraft concepts and studies are discussed. Finally, the issue with high voltage at high altitude is explained along with the use of the High Temperature Superconductors.

2.1. Aircraft Electric Propulsion

As natural resources are being consumed at ever more frenetic rates, environmental preservation has become an increasingly urgent issue. In order to reduce pollutant emissions such as greenhouse gases, a change in human consciousness and current technologies is necessary. Although the aviation sector only emits 1.9% of greenhouse gases worldwide (in 2016 [6]), the fact that these gases are emitted at high altitudes affects the destruction of the ozone layer much more considerably than the pollution of other sectors.

2.1.1. Electric Propulsion Configurations

With now-a-days technology, an aircraft requires between 100 kW (unmanned aircrafts) and 80 MW (largest transport aircrafts such as the Boeing 777) on average for propulsion. If part of this power is to be supplied electrically, the conventional propulsion system must vary in several respects.

Different electric propulsion configurations for aviation applications are proposed and can be used [7]. Although most designs include a gas turbine, an all-electric configuration is also proposed. Four configurations are differentiated: turbo-electric power controlled, hybrid-electric parallel, hybrid-electric serial and the all-electric configuration. The four configurations mentioned above can be found in **Figure 1**.

The turboelectric configuration consists of a gas turbine driving an electric power generator (**Figure 1** (a)). Since this energy is transported by a DC bus, electronic components are needed to transform the alternating current from the generator into direct current and, at the input of the electric motor, an inverter to transform the direct current back into alternating current. The electric motor will be in charge of driving the propeller of the aircraft.

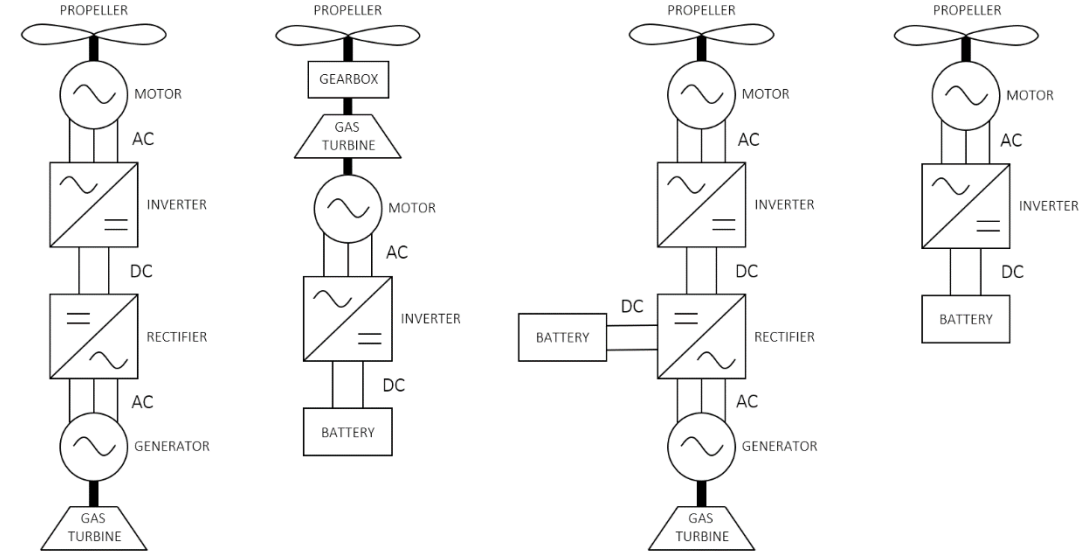

(a) Turbo-electric (b) Parallel Hybrid (c) Serial Hybrid (d) All-electric

Figure 1. Electric propulsion principal configurations.

Hybrid configurations are characterised by the fact that the energy consumed by the engine is partly obtained from a gas turbine (as in the turbo-electric engine), but in this case batteries are also included. The energy stored in the batteries is used during take-off and landing, when the power requirements are the highest, thus reducing the power demanded by the gas turbine.

During cruise, the energy consumed will be obtained exclusively from the gas turbine. The problem with battery models is the fact that they need to be recharged at the airport and this can take a long time. Another option would be to exchange the discharged batteries after the flight for charged ones.

The serial hybrid configuration is very similar to the turboelectric (**Figure 1** (c)). However, it has batteries connected to the rectifier that provide the necessary power to the system. This makes this a very heavy model, which is its major disadvantage. In the case of the parallel hybrid engine, the electric motor is mounted on the same power shaft as the gas turbine (**Figure 1** (b)). The issue with this configuration is that the motor can suffer a temperature rise due to its proximity to the gas turbine.

Finally, the all-electric concept is the simplest (**Figure 1** (d)). Power is supplied by batteries which, through a DC bus, transport the direct current to an inverter. The inverter transforms it into alternating current, which goes directly to the electric motor, and this drives the aircraft's propeller. Although in principle this is the optimum configuration in terms of efficiency and energy consumption, with the values of energy densities that are currently available, the model is not feasible due to the resulting weight of the batteries.

2.1.2. Distributed Propulsion

Most large aircraft have engines placed under the wings in an attempt to be as aerodynamically efficient as possible. However, as the analytical and computational study of aircraft performance has improved in the last decades, new distributions and geometries have been considered, such as the distributed propulsion.

The distributed propulsion provides an increase in the efficiency of the aircraft by different factors. By separating the power generator from the plane's propeller (as can be seen in **Figure 2**), it opens up the possibility of diversifying the thrust in several propellers throughout the aircraft, without the need to have a specific engine for each one, as is the case in conventional turboprop aircraft. In this way, the efficiency of each propeller is increased by the aerodynamic and thermal conditions, achieving higher overall efficiency.

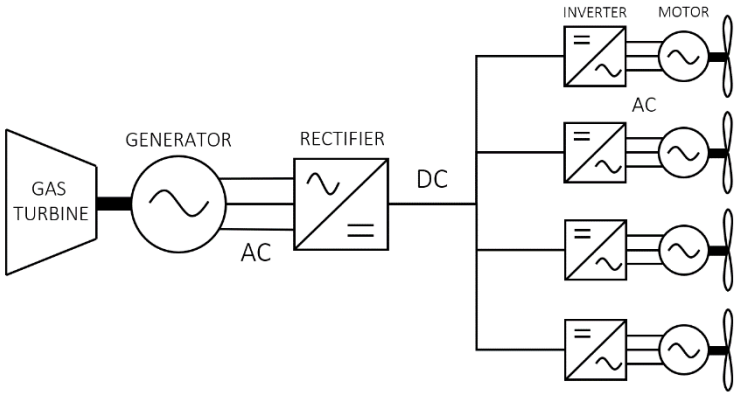

Figure 2. Basic configuration of a 4-motor distributed propulsion.

Along with distributed propulsion, boundary layer ingestion (BLI), a technique that consists of employing the layer of fluid closest to the surface of the fuselage (flowing at reduced speed) to propel the aircraft, is being applied. BLI will be explained in more detail in **2.3.2.1**.

Several investigations have been carried out by different groups about the distributed propulsion, summarized by Berg *et al*. [8], Gohardani *et al*. [9] and Kim [10].

2.2. History of the Electric Aircraft

Since the globalisation of the use of electricity, attempts have been made to replace the combustion engines with electric motors. Although electric motors may seem to be an innovative technology, the initial designs date back to the 1830s. As for their application for aeronautical purposes, the first vehicle to incorporate electric propulsion was 'La France', an airship designed in 1883 [11]. Over the last 140 years, different models have been proposed, but it was not until the 2010s that research into this type of vehicle began to be carried out more intensively.

2.2.1. Earliest Designs. Gliders

The first designs were powered by electric energy obtained from electric panels placed directly on the wings of the vehicles (e.g. the 'Sunseeker' in 1990 [12]). However, the first model to make an official flight was the Lange Antares 20E in 2003 [13] (**Figure 3**). This first manned electric aircraft model is a 20-metre wingspan glider, equipped with a 42-kW electric motor.

Since 2008 every year several concepts, designs and airplanes have been presented, both for sale and on an experimental basis. Most of them were one or two-seater small aircrafts or gliders (e.g. the Electraflyer C [14] and the Yuneec E430 [15]), due to the difficulty of lifting heavier loads with the electrically supplied power.

Figure 3. Lange Antares 20E (Lange Aviation image).

2.2.2. More Powerful Electric Aircrafts. Milestones and larger Companies

Later, new models were developed with the intention of being produced for the public, not only as prototypes or demonstrators (e.g. the Pipistrel Taurus Electro G2 [16] and the Pipistrel Alpha Electro [17]). The first hybrid electric aircraft was the Diamond DA36 e-Star (in collaboration with Siemens) [18]. The purpose of this model was to research the serial hybrid electric drive system on smaller aircrafts or gliders to be scaled later on larger vehicles.

Some other prototypes' aims were to break electric aircraft speed records, e.g. the Long ESA of Chip Yates, which is known for the milestone itself (reaching a top speed of 326 km/h) rather than for making a powerful aircraft [19].

Large firms have also taken part on the growth of the more electric aircraft. Boeing presented the Boeing HK-36 fuel-cell demonstrator in 2008 [20]. Airbus, on the other hand, has continuously developed electric propelled gliders (e.g. the e-Genius [21]), small aircrafts (e.g. the E-Fan 1.0 [22]) and even launched a hybrid-electric aircraft demonstrator for more than 70 passengers (the E-Fan X [23]), which was cancelled due to the drop of air travel caused by the COVID-19 pandemic [24]. However, the company keeps working on the research of the electric propulsion with projects such as the CityAirbus, a four-seat eVTOL demonstrator [25] (**Figure 4**).

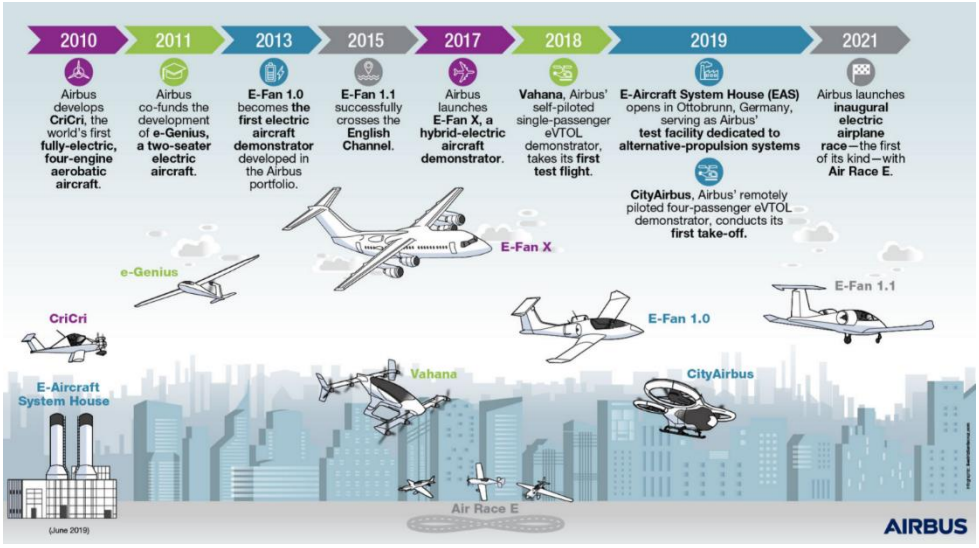

Figure 4. Timeline of Airbus' electric propelled projects (Airbus image).

Siemens, the German multinational and Europe's largest engineering company, is one of the oldest suppliers of equipment for the energy and transport industries. As such, they are one of the world's largest developers of electric motors, and the aeronautics sector is no exception. Although Siemens has also produced its own aircraft (the Siemens Extra 330LE [26], which broke

again the top speed record), there are several prototypes in which the engine used bears the manufacturer's signature. Good examples are the aforementioned Diamond DA36 e-Star (70 kW) and e-Star 2 (80 kW) or the Pipistrel WattsUP (85 kW).

Another company that has also recently joined the electric propulsion research is Ampaire, founded in 2016 (California, USA). It flew its first model, the Ampaire EEL, in 2019 [27].

2.2.3. Latest Flyable Designs. Most powerful EPAC

The most powerful electric aircraft designed to date is the Cessna eCaravan [28], which made its maiden flight in May 2020. This model is a Cessna Caravan 208 whose combustion engine has been replaced by a 560-kW electric motor from MagniX (the Magni500). This motor, which can provide a continuous torque of 2814 Nm, was also used on the Harbour ePlane, a Canadian seaplane that made its first flight six months earlier [29].

However, all the aforementioned models are still far from the range of power and energy capacity of a regional passenger airplane. With the technology available now-a-days, especially in terms of the specific energy of the batteries, it is difficult to envisage that in the medium-term future such larger aircraft will be fully electric-powered. Despite this, several concepts and studies are being carried out at the moment on both new models and new technologies such as high temperature superconducting motors.

Next table (**Table 1**) summarizes the aforementioned manned electric aircrafts along with their pick power, number of seats, the maximum take-off weight and the most relevant highlight of each one of them. Moreover, in **Figure 5**, the aircrafts are plotted depending on the electric power required for each model and, in **Figure 6**, the temporary evolution of the maximum take-off weight is shown.

Table 1

Summary of manned electric aircrafts [1].

1st flight year	Name	Peak power (kW)	Seats	Maximum weight (kg)	Highlights	Ref.
2003	Antares 20E	42	1	660	1st electrical motorglider	[13]
2008	EAC Electraflyer C	13.5	1	283	Small electric motorglider	[14]
2008	Boeing HK-36 FCD	75	1	860	Electric motorglider, fuel cell	[20]
2009	Yuneec E430	40	2	470	Composite electric AC marketable	[15]
2011	DA36 e-Star	70	2	800	1st serial hybrid electric AC	[18]
2011	Pipistrel Taurus Electro G2	40	2	450	2-seater AC commercially available	[16]
2011	Pipistrel Taurus Electro G4	150	4	1500	Two G2 merged, experimental	[30]
2011	IFB Stuttgart e-Genius	60	2	950	University experimental electric glider	[21]
2011	Embry-Riddle Eco-Eagle	105	2	1075	Experimental hybrid AC	[31]

1st flight year	Name	Peak power (kW)	Seats	Maximum weight (kg)	Highlights	Ref.
2012	EAC Electraflyer ULS	15	1	238	Experimental electric aircraft	[32]
2012	Chip Yates Long ESA	192	1	680	All-electric speed-record-breaking AC	[19]
2013	DA36 e-Star 2	80	2	800	Experimental	[33]
2014	Airbus E-Fan	60	2	600	Two 30 kW fans, experimental	[22]
2014	Cambridge SOUL Watts up	20	1	235	Recharges batteries during flight	[34]
2015	Pipistrel Alpha Electro	60	2	550	2-seater AC commercially available	[17]
2016	Airbus E-Fan 1.2	60	2	600	Experimental, similar to 1.0	[22]
2016	Siemens Extra 330LE	260	1	1000	Very efficient, short-travel powerful AC	[26]
2019	Ampaire EEL	160	6	2000	Parallel hybrid electric AC	[27]
2019	Harbour Seaplanes ePlane	560	6	1500	1st electric seaplane commercially av.	[29]
2020	Cessna eCaravan	560	10	2100	Largest electric aircraft to the date	[28]

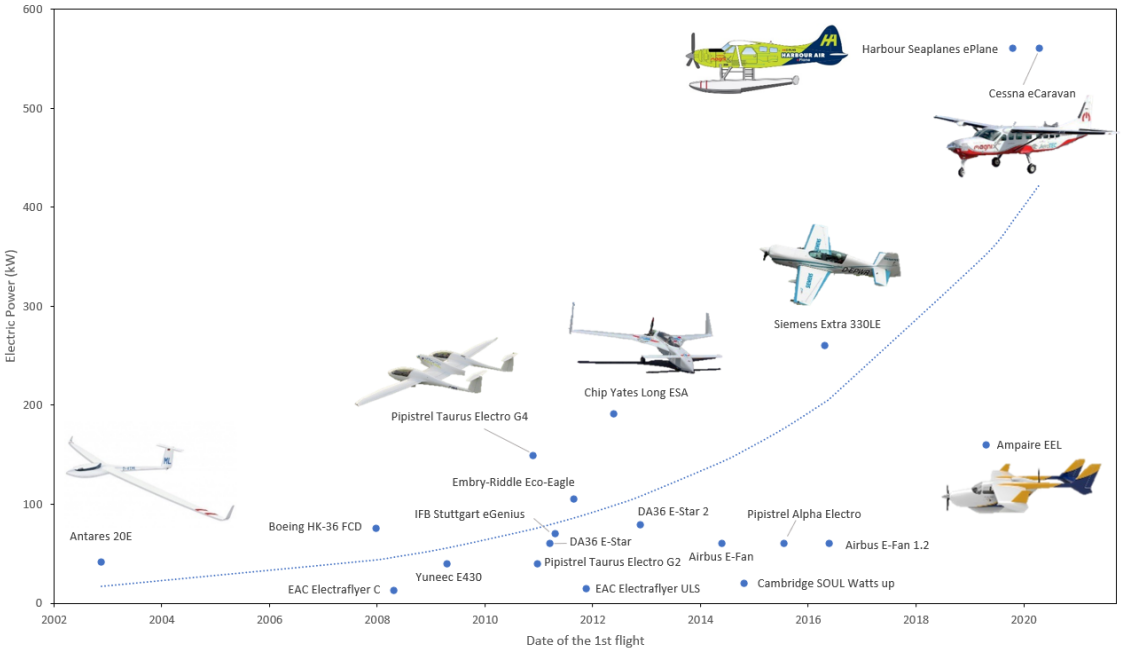

Figure 5. Temporary evolution of electric propulsion power (data from **Table 1**).

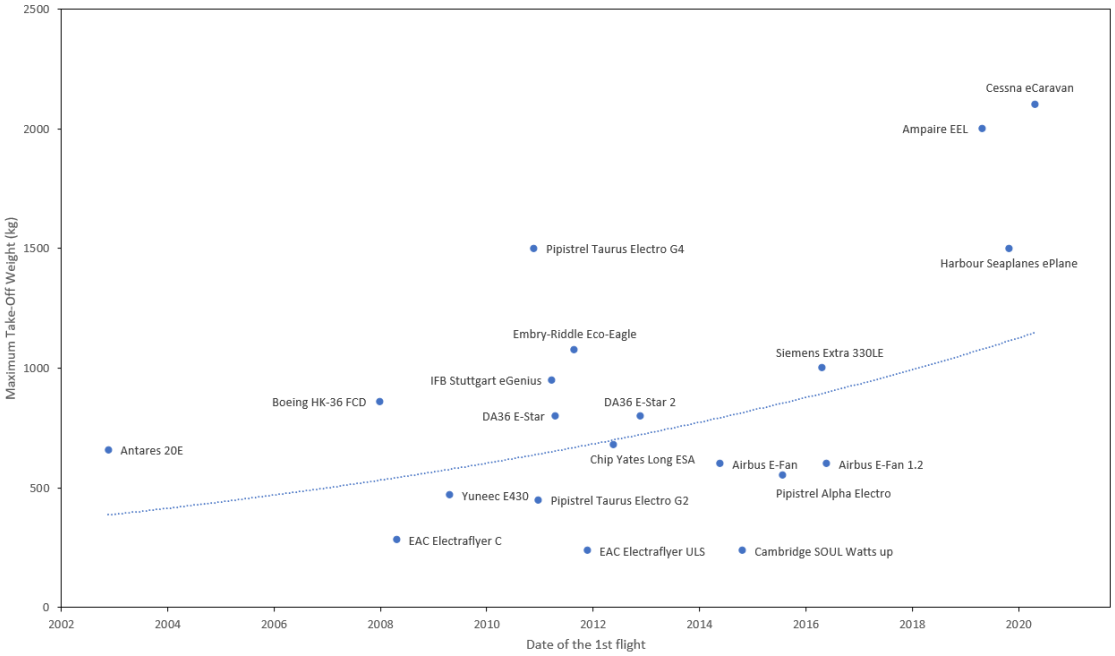

Figure 6. Temporary evolution of maximum take-off weight (data from **Table 1**).

2.3. Electric Aircraft Concepts and Studies

Among the studies currently being carried out, two main distinctions can be made: the models that are expected to make their first flight in the near future (in the 2020s) and the set of concepts and models with a higher technological level that still need to mature in order to become a flyable aircraft.

2.3.1. Short-term Flyable Aircrafts

The model that intends to fly in the shortest term is Rolls-Royce's 'Spirit of Innovation' [35]. This light aircraft from the British firm has been developed to break the speed record for an electric-powered aircraft currently held by the Siemens Extra 330LE with a speed of 337 km/h. The Rolls-Royce model is expected to exceed 480 km/h with a 400-kW engine.

Another aircraft that follows the trend line of those already demonstrated in the previous chapter is NASA's X-57 'Maxwell' [36] shown in **Figure 7**. The X-57 is part of the NASA's Leading Edge Asynchronous Propeller Technology (LEAPTech [37]) project which develops an experimental technology consisting on placing several small propellers along the edge of the wings (distributed propulsion aircraft). With this technology, each motor can be operated independently at different speeds for optimized performance. In the specific case of the NASA X-57, 14 engines are fitted, 7 on each wing. At the wing tip the most powerful engines are located for continuous operation, while the remaining 12 smaller engines are used for take-off and landing, when more power is required.

Figure 7. NASA's X-57 'Maxwell' airplane (NASA image).

Iranian firm Eviation's Alice model is also scheduled to make its maiden flight in 2021 [38]. This aircraft is powered by three MagniX propulsion engines (the Magni250, each capable of delivering a peak power of 280 kW at the base speed of 1900 rpm). Eviation's all-composite Alice is a light aircraft capable of carrying 11 passengers (9 and the two pilots) and is intended to be marketable.

2.3.2. Larger and MW-class Concepts. BLI and HTS Technologies

On the other hand, over the last few years, different projects and studies have been developed with the aim of increasing the power density of aircraft electric motors in order to boost the planes' thrust power. With the intention of flying regional aircraft of more than 150 passengers, groundbreaking technologies such as BLI (boundary layer ingestion) and partially or fully superconducting engines are beginning to be implemented.

2.3.2.1. Boundary Layer Ingestion (BLI)

BLI consists of using the boundary layer of fluid in the airframe directly on one or more of the aircraft's propellers to improve the fuel efficiency of the propeller. Although this type of technology has already been used in other areas such as ships or missiles, BLI is not common in aircraft [39].

Although BLI is a resource that can be used in any type of aircraft (without the need for electric propulsion), it is of particular interest in more electric aircraft due to the improvements in efficiency that it brings. Since electric propulsion is still a mature area, it is being optimised as much as possible, and BLI can help to advance in this field.

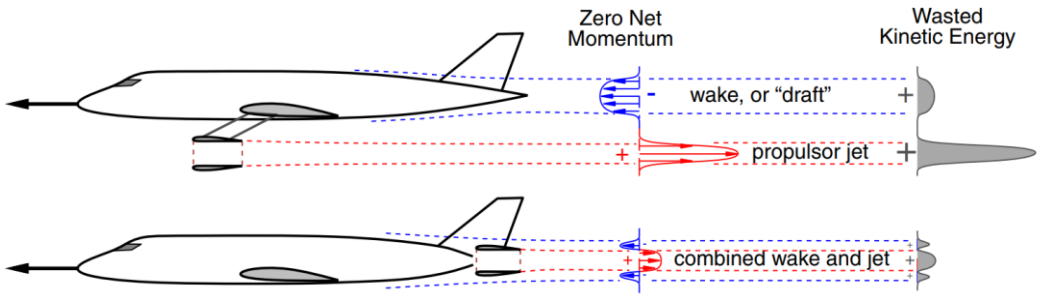

Figure 8. Illustration of the wasted kinetic energy comparison between a conventional aircraft (top) and an aircraft with BLI (bottom) [40].

Even considering the improvement in efficiency brought about by this technology, the fact that the air flow entering the propeller is not uniform in pressure distribution (as it is in a standard propeller) has a negative effect on the propeller's mechanics.

The optimum position for a BLI propeller on a traditional airframe aircraft is at the tail of the aircraft. In this way, it takes advantage of the boundary layer of the fluid flowing along the aircraft to optimise propulsion. Examples of this arrangement are the Ampaire Tailwind [41], NASA's STARC-ABL [42] and Airbus' VoltAir [43] (**Figure 9**).

Figure 9. BLI at the tail of the Ampaire Tailwind (Ampaire image).

However, research into electric propulsion is leading to the redesign of conventional aircraft, giving rise to novel geometries and designs, as in the case of Airbus' E-Thrust [44] or NASA's N3-X [45], models that employ disruptive designs that allow BLI propellers to be placed along their wings, with the same effect, and thus optimise the demonstrator's efficiency.

2.3.2.2. Superconductivity

Another groundbreaking new technology is superconductivity in electric motors. Within this topology, it is possible to find partially superconducting motors (with a superconducting rotor or stator) or completely superconducting motors. Superconductivity manages to reduce the electrical resistance to practically zero, thus achieving high current densities with a relative low voltage [46].

This technology results in lighter electric motors (in the case of partially superconducting motors) and up to 3 times lighter (in the case of fully superconducting motors) than equivalent conventional motors [47]. In addition, due to both the aforementioned weight reduction and the increased flux density in the air gap, much higher power density values are achieved

compared to motors of similar performance. Moreover, with zero-resistance conductors, power losses are considerably reduced.

Even if HTS is a great option to consider for the development of all-electric aircraft, these types of superconductors require a cryogenic temperature for their operation. The feasibility of the superconducting motor depends on the cryocooling system, a system that requires power and therefore consumption in addition to that of the motor. A considerable alternative could be the use of hydrogen both as a fuel and as cryocooler, a technology that is on constant research. The topic of the high temperature superconductors (HTS) will be discussed on the following chapters.

In the following table (**Table 2**), the current electric aircraft concepts and studies are summarized. Moreover, the **Figure 10** represent the expected electric power required for each of the aircraft mentioned.

Table 2

Summary of electric aircraft concepts and studies [1].

1st flight year	Name	Peak power (kW)	Seats	Maximum weight (kg)		*Ref.*
2021	RR Spirit of Innovation	400	1		Intended to break the speed record	[35]
2021	Eviation Alice	900	11	6350	9 passenger electric AC, 3 propellers	[38]
2020s	NASA X-57 'Maxwell'	246	2	1360	2x60 and 12x10.5kW propellers	[36]
2020s	Ampaire Eco Otter SX		19		Hybrid-electric 19-seater	[48]
2020s	Ampaire Tailwind	1000			Tail-mounted BLI propeller	[41]
2020s	Zunum Aero	1000	12	5216	Similar to Alice, delayed by Boeing	[49]
2024	XTI Tri-Fan 600	1500	6	2400	VTOL with fixed wings	[50]
2035	NASA STARC-ABL	2600	154	60000	Single-aisle Turboelectric AC, BLI prop.	[42]
2035	Boeing SUGAR Volt	1000	154	68040	Strut-braced wing w/+150 passenger AC	[51]
2035	Bauhaus Luftfahrt Ce-Liner	33500	189	109300	C-wings, superconductive, risky tech.	[52]
2035	Airbus VoltAir		33	33000	BLI, superconducting, long-term	[43]
2035	ESAero/Wright ECO-150R	12700	150	60000	16 propellers on the wing, no supercon.	[53]
2045	NASA N3-X	50000	300	227000	BLI, superconducting distributed motors	[45]
2050	Airbus/R-R E-Thrust		90		BLI, superconducting embedded fans	[44]

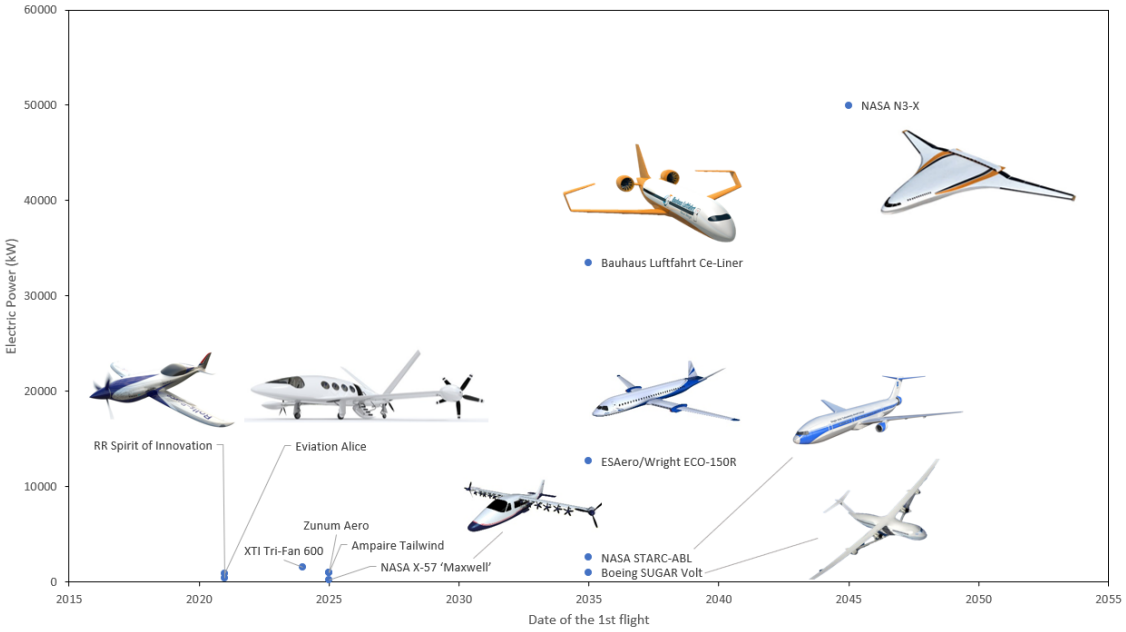

Figure 10. Ongoing studies and projects of electric propulsion (data from **Table 2**).

2.4. High Voltage Electrical Systems at High Altitude

High voltage systems have various purposes such as transformers, high power equipment, insulation testing of cables and capacitors and, above all, transportation of energy over long distances with as low losses as possible. Nevertheless, all these applications do not require specific atmospheric conditions of pressure and temperature, due to the altitude at which the aircrafts operate. Therefore, there are not many studies on the implementation of a high voltage system in an aircraft.

Work has been developed around the Paschen Curve (**Figure 11**), which relates the air pressure at which a conductor is found and the partial discharge inception voltage (PDIV). According to this curve, when the atmospheric pressure is reduced, the limiting value at which partial discharges occur due to voltage breakdown also decreases to a minimum value. This is why such a system requires further study of the insulation of conductors and electrical machines working at cruising altitudes of the range of 10,000 to 15,000 m.

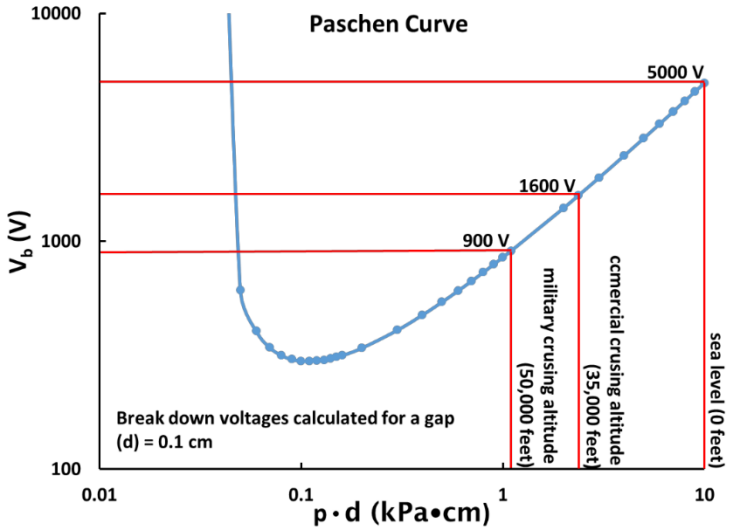

Figure 11. Paschen Curve for the case of two parallel plates [86].

Despite the fact that the Paschen Curve can approximate the value of the partial discharge inception voltage for a given ambient pressure, the curve is only valid for a certain type of material, conductor geometry and conditions. The resulting curve depends on the condition of the model and it may vary drastically. Regarding the specific case of the electric airplanes, there is currently not much work on the subject and this is why it should be studied thoroughly to advance on the development of the electric aircraft.

Moreover, the issue with electrical discharges and high voltage arcing events is that it is very difficult to mitigate them once they have started, thus leading to catastrophic results. For this

reason, it is particularly important in the case of electric aircraft to ensure that the electrical insulation of the conductors is well secured and modelled.

Regarding partial discharges in inverted-fed electric motors at low pressures, Cavallini *et al.* have done some remarkable work, with an approach partly directed at electric propulsion of aircraft [54], [55]. However, the modelling of this phenomenon is poor, limited to a pair of twisted wires and, therefore, very low voltage systems [56].

2.5. High Temperature Superconductors (HTS)

Although there are ongoing studies on superconductors, the technology is not very mature yet. However, it is a system that has many advantages and, once developed, would help significantly in the move towards all-electric aircraft. Superconductors are feasible both in the electrical distribution of the aircraft and in its motors' windings.

2.5.1. Electrical Energy Distribution

There are several ways to make the electrical distribution of an aircraft. Specific studies about aircraft's electrical distribution were made by Berg *et al.* [8].

On the one hand, alternating current power distribution can be considered. With this type of distribution, the losses in the copper are considerable, but a reduction in the frequency of the current would help to reduce the losses in this type of electrical distribution. However, this would require power electronics which, again, implies a reduction in system performance and increases the total weight.

On the other hand, DC distribution is the most logical choice since the copper losses are much lower than in the case of AC distribution. However, the rectifier and the inverter have to be considered both because of the losses and the increased weight caused by these power electronics devices. Working with high voltages would reduce electronic losses but would require more insulation in the conductors to avoid partial discharges caused by the high voltage. Lusuardi *et al.* [54] and Hayakawa *et al.* [56] (**Figure 12**) have studied the partial discharge on conductors even if the work available regarding this topic is limited.

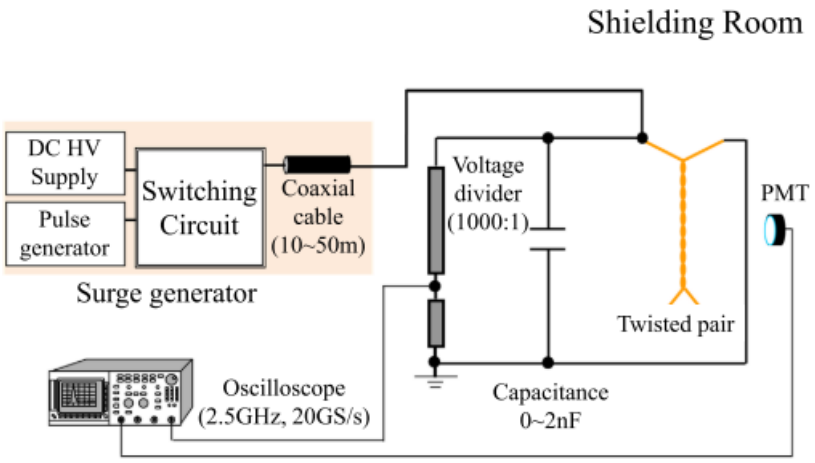

Figure 12. Scheme of the study of partial discharge on conductors by Hayakawa *et al.* [56].

By the use of superconductors, high currents can be achieved at lower voltages due to near zero resistance. The issue with superconductors is that they only operate at cryogenic temperatures, and therefore the increased weight and extra power consumption that such a cooling system would require must be considered.

2.5.2. Electrical Machines

Superconductors can also be used in the motor winding. The optimal and most efficient configuration would be to use superconductors in the field and in the armature of the motor. However, with today's technology, most electrical machines that use superconductors do so only in the field winding as it is less technologically complex even though the potential is more limited than using HTS in the rotor and stator [8].

A number of motors and generators have been developed over the last few years although most of them were not for aviation applications. The vast majority of designs were intended for sectors with high torque and low speed requirements such as wind turbines or motors for large ships. An example of this kind of HTS motors are the 10-MW-class wind turbine HTS synchronous generator analysed by Shafaie *et al.* [57] or the also 10-MW-class wind turbine HTS wind generator coil designed by Sarmiento *et al.* [58] (**Figure 13**) and the 3-MW HTS motor for ship propulsion developed by Yanamoto *et al.* [59].

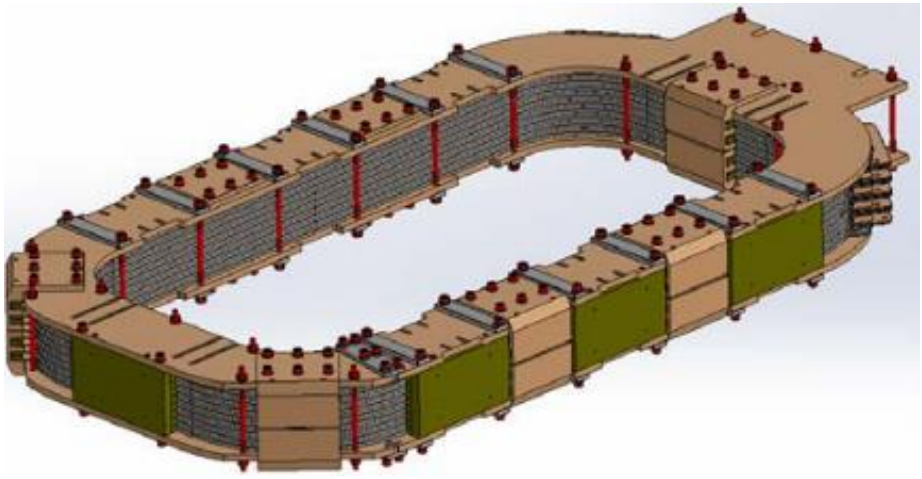

Figure 13. 10 MW generator field coil designed by Sarmiento *et al.* [58].

Aircraft motors, on the other hand, are characterised by high speed and low torque, so there are not as many models or studies of aircraft motors using superconductors yet. Nevertheless, some considerable work has been done by a number of authors such as Zhang *et al.* in [60], [61] (**Figure 14**) or by Luongo *et al.* in [47].

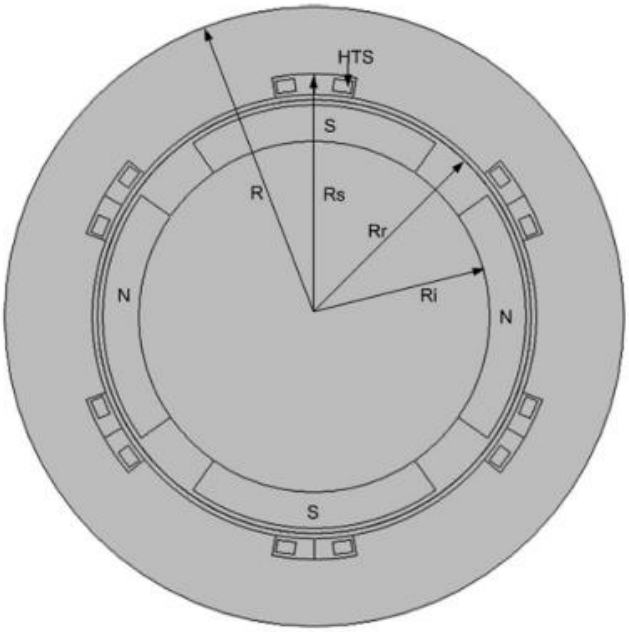

Figure 14. Radial view of 1-MW propulsion motor designed by Zhang *et al* [60].

2.5.3. HTS Materials

Even if the superconductivity phenomenon was discovered in 1911, the potential of the materials with this capability was comprehended almost 40 years ago, along with their disadvantages. Until 1987 the most employed superconducting materials were the NbTi and the Nb_3Sn with a superconducting transition temperature of 10 and 18 Kelvin degrees respectively. Nevertheless, from 1987 the superconducting critical temperature increased notoriously due to the discovery of layered cuprate superconductors (values up to 100 K) [62]. Despite their high cost, complicated implementation and other obstacles, various models and prototypes have been developed in the meantime that feature this technology.

Nowadays several superconducting materials can be found and they can be split and two main groups: low temperature superconductors (LTS) and high temperature superconductors (HTS). The materials on the first category are used in more classical applications such as particle accelerators or magnetic resonances that do not require high frequencies, whereas the newer high temperature superconductors are used for electric power equipment such as motors [63], generators [57] or power transmission cables [64]. Nevertheless, according to the BCS theory of superconductivity proposed in 1957 (named after Bardeen, Cooper and Schrieffer), there is no upper limit to the value of the critical superconducting temperature; all is needed is a favourable combination of high-frequency phonons, strong electron-phonon coupling, and a high density of states [65].

There are hundreds of material alloys that are capable of being superconducting at conditions below the critical superconducting temperature. However, only a few are suitable for aeronautical applications due to the specific conditions to which they must be exposed. The most commonly used superconducting wire is the aforementioned NbTi, but as it is LTS it does not make sense to use it in electrical machines where a large cryocooler required to superconduct electricity would reduce the efficiency [62]. Although Nb_3Sn has a slightly higher critical temperature, it is difficult to manufacture for being a ceramic compound [66].

The metal alloy MgB_2 is a relatively inexpensive alternative capable of working at medium-high temperatures (up to 40 Kelvin degrees) [67]. Moreover, having a simple crystalline structure, large coherence lengths and high current densities, this inorganic magnesium compound is of particular interest for large-scale applications (**Figure 15**).

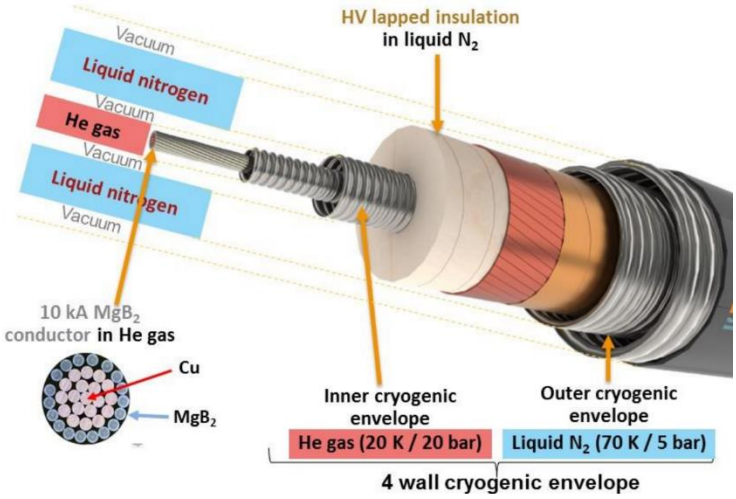

Figure 15. MgB_2 wires for superconducting cable demonstrator.

In the late 1980s, new superconducting materials called second generation (2G) HTS were developed. These materials are composed of cuprate and other metals such as bismuth (BSCCO) [62], yttrium (YBCO) [68] or lanthanum (LBCO) [69]. Some of these alloys are capable of reaching critical superconducting temperatures of up to 108 Kelvin, as in the case of Bi-2223 [70]. The complex manufacturing process of these materials makes them expensive, though the use of high operation temperatures may reduce the overall cost. Several electrical machines have already been developed using these second-generation superconductors.

The critical temperature reached a value of 135 Kelvin degrees in 1993 by studying a new cuprate, Hg-1223, a material of the HBCCO family [71]. Twenty-two years later, in 2015, the critical temperature record for superconductivity in a material was broken again, with a value of over 200 K [72]. In this case, thanks to research on hydrides, H_2S was able to behave as a superconductor at a pressure of more than 150 GPa. Although the critical temperature is

becoming progressively closer to the ambient temperature, auxiliary systems are required in order to obtain the specific environmental conditions for superconduction to occur. Therefore, at least until this technology matures and is further developed, it is not efficient to use such superconductors in aviation applications.

On the next table (**Table 3**) the aforementioned materials are shown along with their critical temperatures. Also, in **Figure 16**, the temporary evolution of the critical temperature of the different superconductors is plotted.

Table 3

Summary of superconducting materials.

Structure	Year	T_c (K)	Class	Ref.
Nb_3Sn	1954	18	Compound	[66]
NbTi	1962	10	Compound	[62]
LBCO	1986	35	Cuprate	[69]
YBCO	1986	93	Cuprate	[68]
Bi-2201 (BSCCO)	1988	33	Cuprate	[73]
Bi-2212 (BSCCO)	1988	86	Cuprate	[74]
Bi-2223 (BSCCO)	1988	108	Cuprate	[70]
Hg-1223 (HBCCO)	1993	135	Cuprate	[71]
MgB_2	2001	39	Compound	[67]
H_2S	2015	203	Compound	[72]

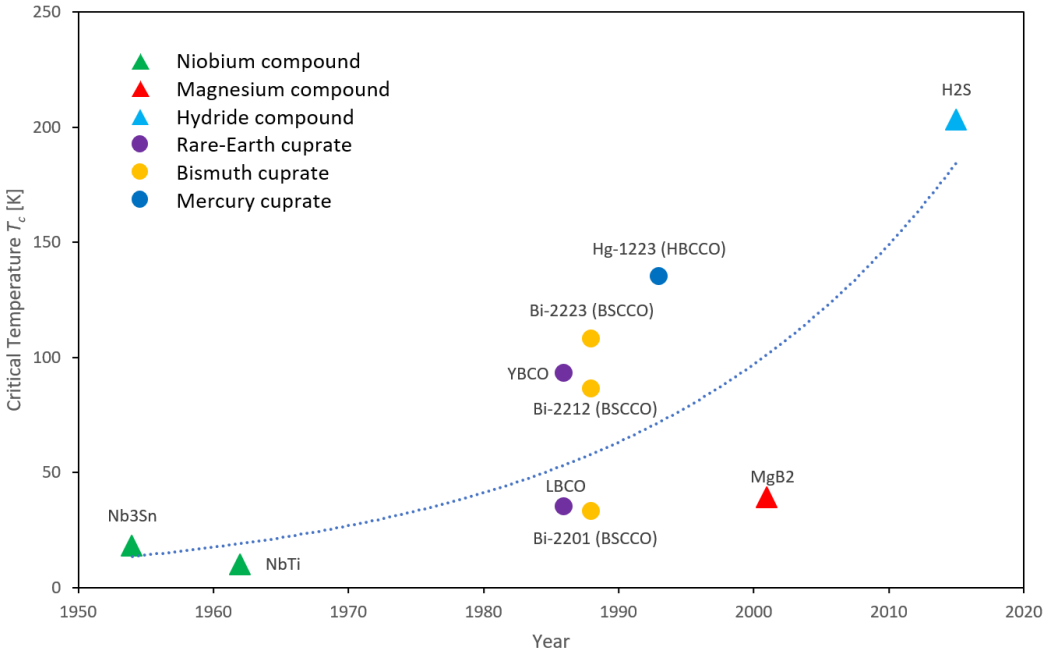

Figure 16. Timeline of the discovery of different superconducting materials (data from **Table 3**).

2.6. Conclusions

Considering every aforementioned discussion and comparison, some requirements have been defined in order to achieved the expected aims. These requisites are divided in four groups: electromagnetic requirements, volume requirements, HTS motor topology requirements and cryogenic cooling system requirements.

2.6.1. Electromagnetic requirements

2.6.1.1. Output power

The electromagnetic requisites are defined by the E-Fan project, which pointed to a motor with a 3000 V_{DC} electrical distribution scheme, as can be seen in **Figure 17**, in order to replace one of the four turbofan engines by a 2 MW electric motor.

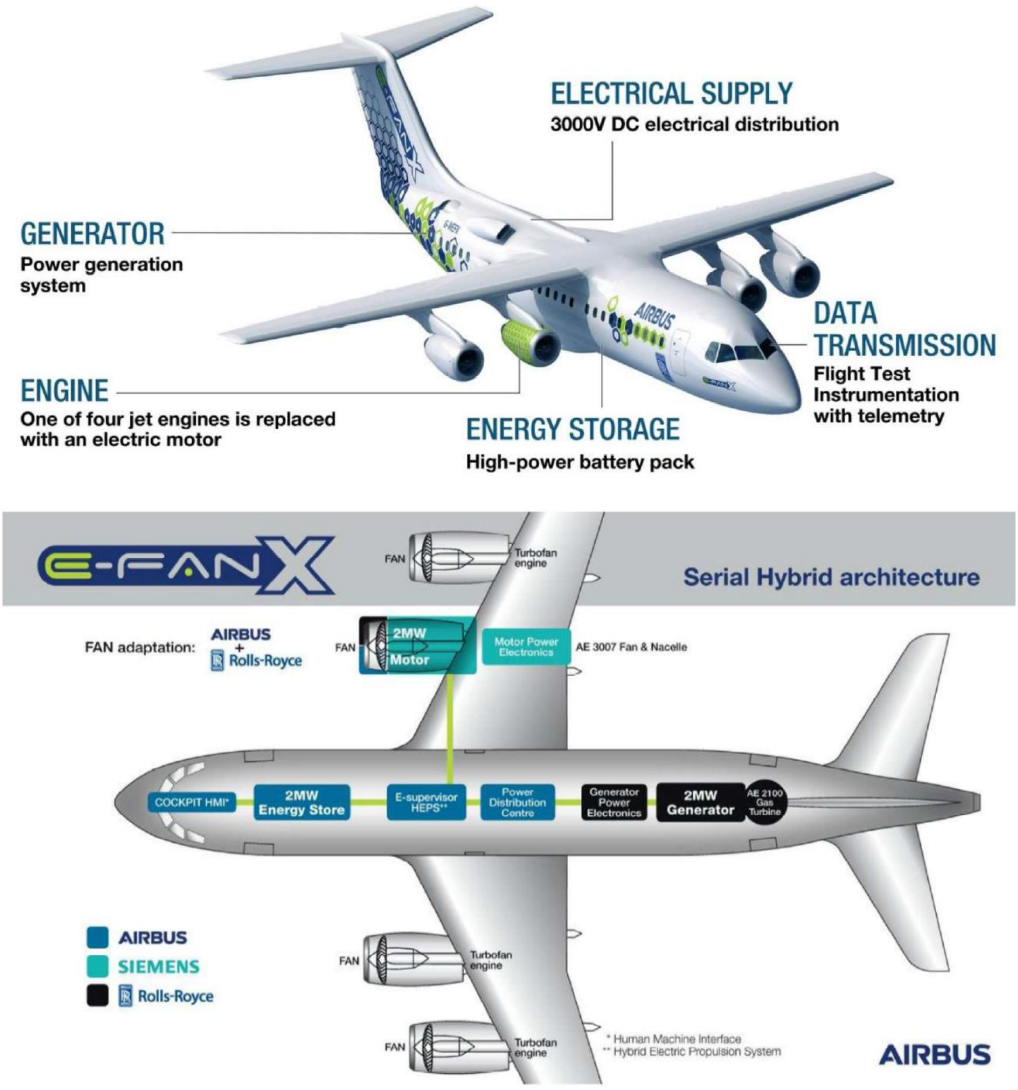

Figure 17. Main features of the E-Fan-X test aircraft obtained from the call.

2.6.1.2. Rotational speed

As it was mentioned in **2.1.1**, the optimum configuration is the serial hybrid-electric, an arrangement where the motor is directly attached to the propeller, leading to rotating speeds of around 2500-4000 RPM. In addition, Jaime Fernandez (member of the EAB, from ITP Aero [75]) recommends setting a 2700 RPM rotation speed for a 3-meter fan.

2.6.1.3. Power density and efficiency

Next table (**Table 4**) shows some of the electric motors for aircraft propulsion developed in the last years with a power density higher than 2 kW/kg. Other projects and studies have developed higher power, superconducting motors; nevertheless, these motors' mass overweight the requirements.

Table 4

Electric motor concepts developed for aircraft applications.

1st flight year	Name	Machine type	Peak power (kW)	Power density (kW/kg)	Rotational speed (RPM)	Efficiency (%)	*Ref.*
2015	SUGAR Volt	SRM	-	4	2500	92	[76]
2018	Siemens SP70D	PMSM	70	2.69	2600	-	[77]
2015	Siemens SP260D	PMSM	260	5.20	2500	95	[77]
-	Siemens SP260D-A	PMSM	260	5.91	2500	95	[77]
-	Siemens SP2000D	PMSM	2000	7.66	6500	-	[77]
2019	magnix250	PMSM	280	3.94	3000	>93	[78]
2019	magnix500	PMSM	560	4.21	2600	>93	[78]
2019	NASA GRC	Part. SC	1400	16	6800	98	[79]

As is shown, the main competitor for superconducting technology seems to be the Permanent Magnets (PM). Considering the previous table, the following goals are proposed:

- Power density: between 7.7 kW/kg and 15 kW/kg.
- Overall efficiency (cooling system included): >=95 % (at nominal conditions).

2.6.1.4. Power converter requirements

For a proper design of an electric motor, it is vital to determine the main features of its controller (power converter).

One of the key parameters for the design of electric motors is the switching frequency, which is constantly increasing as the technology related to semiconductors evolves. An initial value of 30 kHz seems reasonable looking at some of the latest research in this field [80], [81].

In addition, there are more parameters of interest for the design of the electric motor, such as:

- The switching strategy (E.g. SV-PWM, etc.)
- Maximum phase current of the converter (A).
- Maximum phase voltage of the converter (V).
- Voltage variation over time dV/dt (kV/s)

Therefore, the parameters shown in **Table 5** are defined regarding the power electronics governing the electric motor. V_{DC} parameter is an established requirement in the call, and HIVOMOT will study solutions to such high voltage in altitude.

Table 5

Main features of the power converter.

Parameter	Value	Units
VDC	3000	V
Switching frequency	30	kHz

2.6.1.5. Summary

To sum up, **Table 6** shows the electromagnetic requirements defined previously.

Table 6

Electromagnetic requirements.

Parameter	Value	Units
Output power	2	MW
Rotational speed	2700	RPM
Efficiency	>95	%
Power density	7.7-15	kW/kg
V_{DC}	3000	V
Switching frequency	30	kHz

2.6.2. Volume requirements

The electric motor must be designed according to some specific volume/dimension limitations. So, as this topic is focused on the E-Fan project, the volume requirements will be oriented to regional aircraft topologies. In this sense, the volume requirements will be dependent on the nacelle and fan dimensions.

2.6.2.1. Propulsion in regional aircrafts

To delimit the electric motor external dimensions (diameter and length), special attention should be paid on the nacelle and fan characteristics. Regardless of the propulsion system, the nacelle can be defined by some global dimensions, which are depicted in the next figure (**Figure 18**).

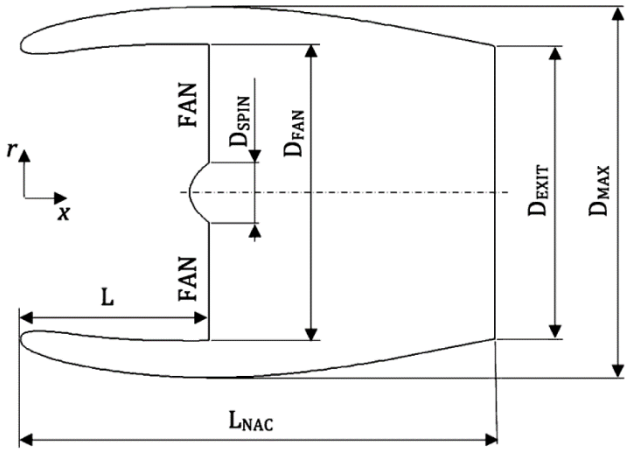

Figure 18. Nacelle cross section with global dimensions in a ducted fan [82].

With these constraints in mind, the propulsion system should be designed according to three key parameters:

- The fan diameter (D_{FAN}).
- The diameter of the spinner (D_{SPIN})
- The length of the nacelle (L_{NAC})

For the fan diameter, [82] proposes a D_{FAN} of 3.3 m for a mid-to-long-range aircraft as a reference value for his study. Therefore, a fan diameter of 3 m seems reasonable for a regional aircraft.

The spinner's diameter is usually between 20-30% of the fan diameter (D_{FAN}). Therefore, taking the D_{FAN} value of 3 m as a reference, the spinner diameter could be set between 0.6-0.9 m.

The length of the nacelle can be defined from either, the fan diameter to length ratio (L_{NAC}/D_{FAN}) or the spinner diameter to length ratio (L_{NAC}/D_{SPIN}) based on previous research.

In addition, [83] shows different motor displacement within the nacelle, as can be seen in the next picture.

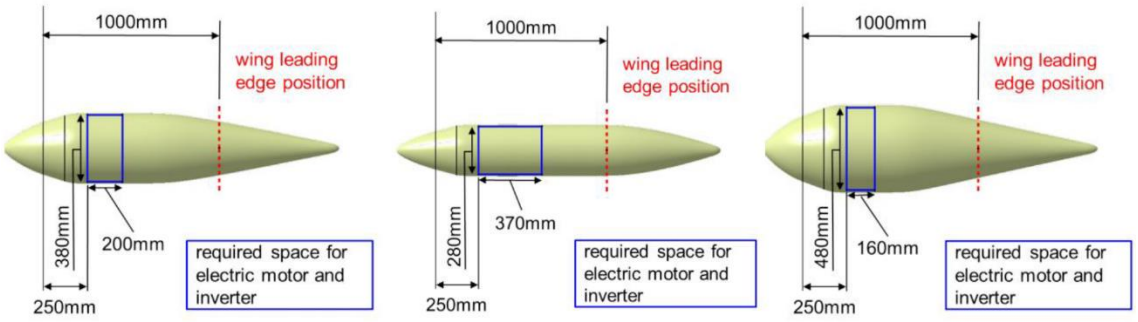

Figure 19. Visualized nacelle geometry for different nacelle diameters [83].

So, from the previous information and looking at **Figure 19**, an available nacelle length (L_{NAC}) of 1 m is considered.

2.6.2.2. Summary

In the previous section, the main dimensions of the propulsion system in a regional aircraft were defined and are summarized in the next table (**Table 7**).

Table 7

Main dimensions of the propulsion system in a regional aircraft.

Parameter	Value	Units
Fan diameter	3	m
Spinner diameter	0.6-0.9	m
Nacelle length	1	m

Considering these dimensions, as the electric motor will be embedded in this system, the following dimensions are proposed for the design:

- Maximum electric motor external diameter: 0.9 m.
- Maximum length for the propulsion system: 1 m.
- Electric motor weight: 130 – 260 kg.

2.6.3. HTS motor topology requirements

One of the most important decisions to be taken when an HTS motor needs to be designed is whether the machine will be partially or fully superconductor. That means that the two components in the motor (rotor and stator in a rotary machine) can, in theory, be superconducting. The compacity of this topology fully superconducting will be maximum.

However, there are practical reasons hindering the selection a fully superconducting machine. The AC losses in the inductive part, which is typically the stator. AC losses in a superconductor penalty the heat load and therefore the cryogenics.

Secondly the study in HIVOMOT of the high voltage in the stator. In a HTS stator the use of high voltage is not necessary.

Thirdly, the time to reach the market. HIVOMOT consortium considers the strategy of reduced innovations in a new technology, trying to fit it to standards. Therefore, HIVOMOT solution intends to be an intermediate step.

The selection of synchronous motor topology has the advantage to work the field winding in DC, avoiding the AC superconductor losses, at least in a first approximation (AC ripples over the DC signal can cause still some AC losses, despite they are usually negligible).

The complete chosen topology is summarized in the following table (**Table 8**).

Table 8

Preliminary motor topology.

Type of motor	Partially superconducting synchronous machine
Superconducting part	*DC Field windings*
Superconducting material	Superconducting wires (2G HTS or MgB2)
Cryogenic parts	*Preliminary Internal rotor (cryogenic rotary joint) or external stator (split rings and brushes)*

2.6.4. Cryogenic cooling system requirements

The next table summarized by Suprasys (**Table 11**) shows the chosen working parameters and systems for the motor.

Table 9

Preliminary motor topology.

Working temperature	20-25 K
Working pressure	*0.1-2 MPa*
Working cryogen	GHe
Cryogenic system	Stationary cryocooler or LH2 heat exchanger with working fluid circulation
Thermal insulation system	Actively cooled radiation shield at around 77 K
Cooling power	40-60 W at 20 K 200 - 300 W at 77 K

Chapter 3

HTS Electric Motor Design Module

As stated in the state of the art given in the previous chapter, new technological breakthroughs are needed to progress on the development of the more electric aircraft. One of these advancements is the use of superconductors to achieve higher magnetic fluxes in the air gap and, in turn, higher power densities than conventional motors. For this reason, a computer program for the design of electric motors with superconducting windings has been developed for this project.

3.1. IPED®

Within the research group of Electric Vehicle at *Ceit BRTA*, a MATLAB-based program called IPED® has been developed over the years with different modules depending on the different types of electric motors analysed. This tool provides accurate electromagnetic and thermal performance results for several modules such as induction motors (IM), permanent magnet synchronous machines (PMSM) or salient pole synchronous machines (SPSM). Nevertheless, due to the immaturity of the technology and the low implementation, a superconducting machine module has never been developed on IPED®.

IPED tool is based on a multi-static magnetic solver which uses the finite element analysis to get the different electromagnetic and thermal outputs of the motor with an open-source program called FEMM® (Finite Element Method Magnetics) [84].

3.2. HTS Module

On this chapter the proposed electromagnetic method for the electric machines' design and calculation is assessed along with its implementation in the IPED® software.

The chosen motor is a salient-pole motor with superconducting winding and slotless stator (**Figure 20**). The salient pole configuration has been selected due to the employment of superconducting winding. On the other hand, the reason of the use of a slotless stator is to let as much space as possible to the stator winding and to reduce the cogging torque. However, a non-conducting divider is used to tie the copper coils (**Figure 21**).

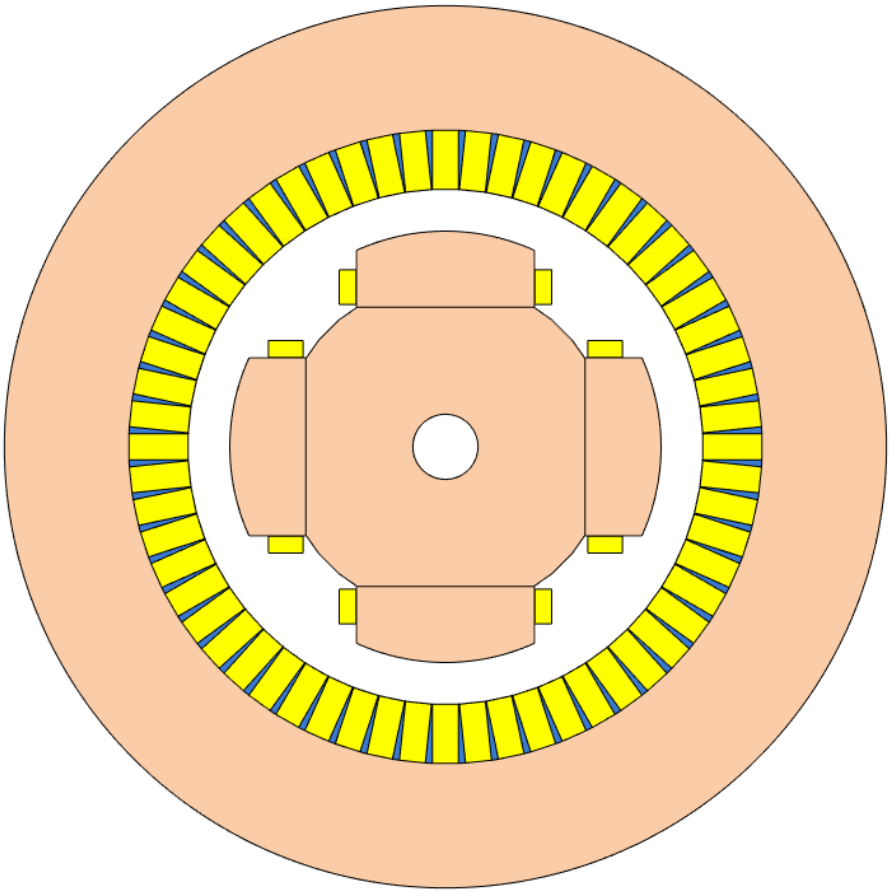

Figure 20. Frontal section of the proposed HTS motor.

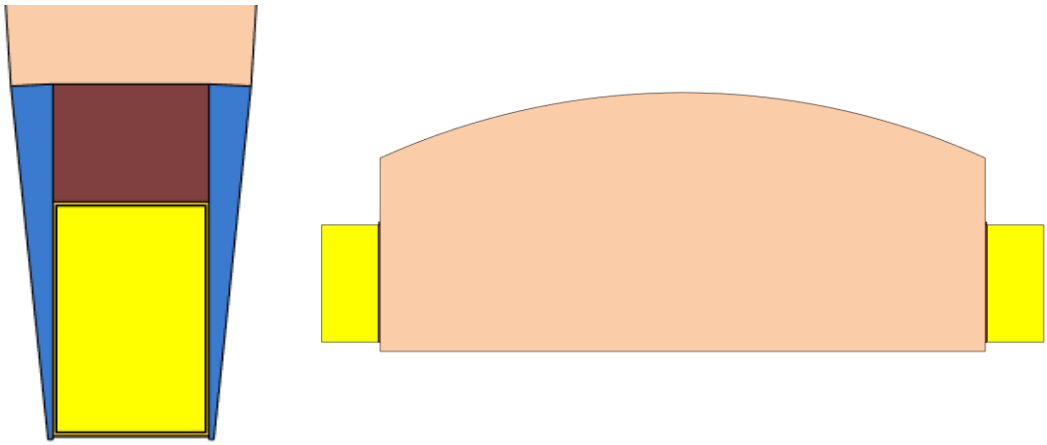

Figure 21. Detail of the stator (left) and rotor (right) winding.

3.2.1. Structure of the HTS Module

The structure of the HTS module is shown in the following block diagram (**Figure 22**) so it can be understood on a simple and comprehensive way. After that, every individual block is explained along with the results that are obtain in each one of them.

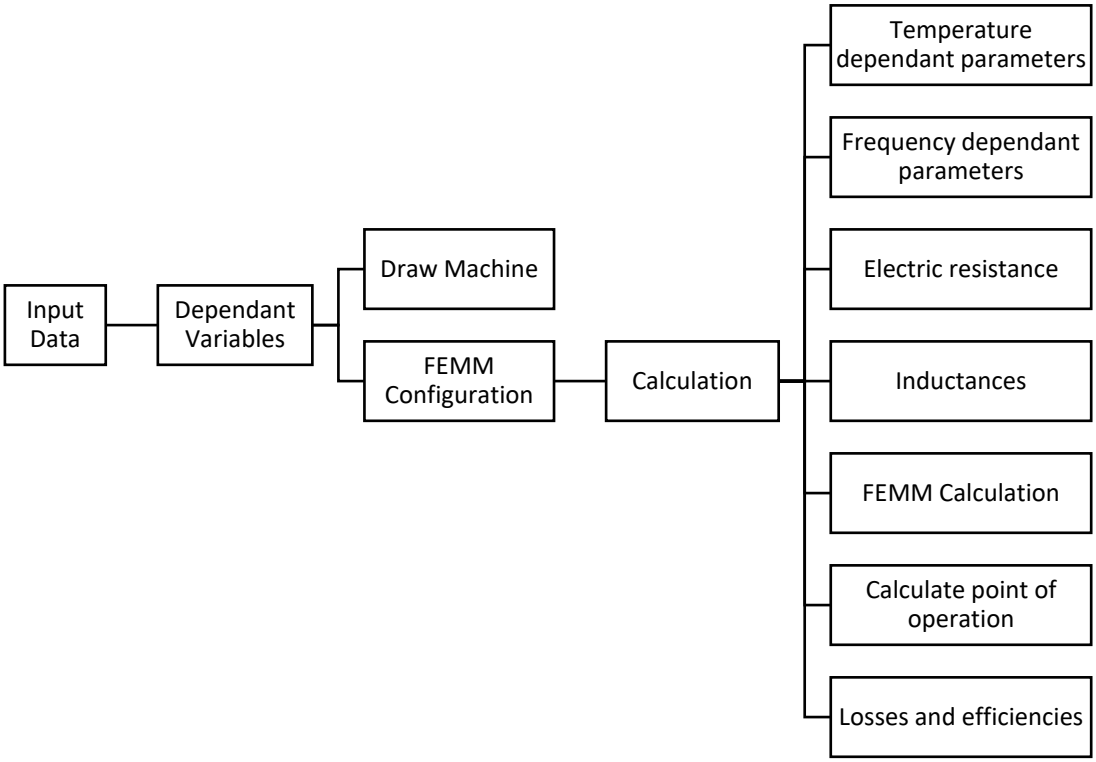

Figure 22. HTS Module structure.

3.2.1.1. Input Data

In order to calculate the superconducting motor some parameters should be defined. Some of them are machine 'inputs' such as the DC Bus Voltage; nevertheless, a number of 'machine

output' parameters are to be defined here such as the output power. The whole input data list can be found below:

- Type of machine (motor or stator).
- Output power [W] or shaft power as the designed machine is a motor.
- Power factor.
- Rated voltage [Vrms].
- Rated rotational speed [RPM].
- Rotor DC current [Arms].
- Motor control criteria ('I_q' in this case).
- The geometry, materials, temperature and winding of the stator.
- The geometry, materials, temperature and winding of the rotor.

The geometric parameters that have to be defined are the number of rotor poles and their size, number of stator slots and their size, inner and outer rotor and stator diameters and the airgap diameter. On the other hand, both rotor and stator windings are to be described: conductor type and shape, number of paths and layers and coil turns.

3.2.1.2. Dependant Variables

After every single input parameter is defined, the different dependant variables are calculated. The independent variables can be classified in seven groups: materials, stator, rotor, insulation, winding, weight and cooling, as can is shown in the following block diagram (**Figure 23**).

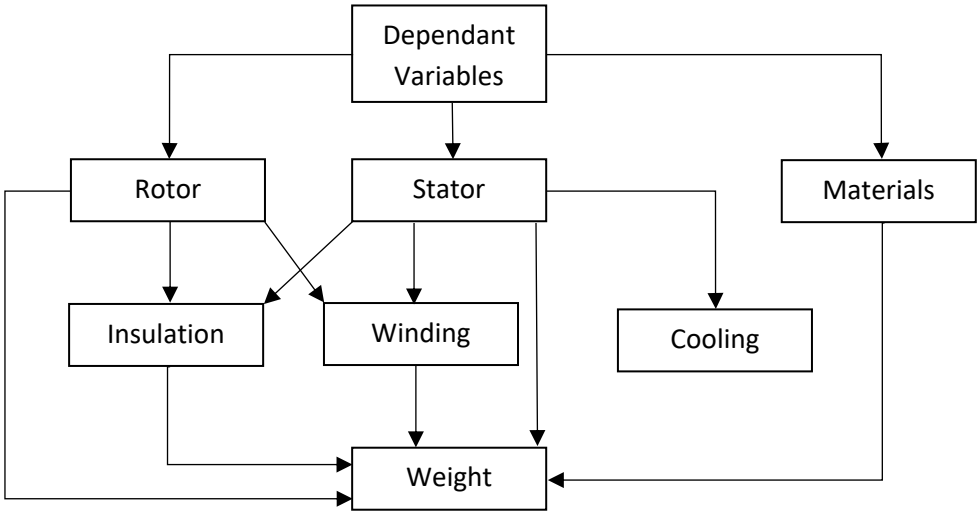

Figure 23. Relation of the dependant variables of the model.

First of all, the properties of the materials are described, according to the materials assigned previously to each part of the machine. The properties that are defined are the specific weight, the lamination thickness, electrical and thermal conductivity and specific heat for the lamination

materials and the specific weight, electrical and thermal conductivity, specific heat, reference temperature and temperature coefficient for the winding materials.

After that, the dependant variables of the stator are specified. For this part, the type of slot is required and, as it was mentioned, the type of slot that has been chosen for the HTS motor is the slotless. Different parameters are calculated for the stator such as the diameters, heights, widths, areas and volumes of the stator slots and the stator yoke and also the exact coordinates are to be defined.

The case of the rotor is similar to the stator. In this case, the type of rotor is, as it was explained previously, a salient pole rotor. With the given rotor inputs different dependant variables are calculated such as the yoke inner and outer diameter, the pole and pole tip width and depth, the areas and volumes and the coordinates of the whole rotor.

The insulation and the winding of both the rotor and the stator are described. The insulation depends on the rated voltage applied to the motor while the winding is function of the input parameters of the winding definition on the 'input data' section.

Even if the cooling dependant variables script has been defined, it will not be explained yet as for the predesign has not been considered any thermal calculation.

Finally, with all the aforementioned information, the total weight of the machine is calculated, considering the rotor and stator lamination and winding as well as the insulation with the specified densities of the materials.

3.2.1.3. Machine drawing

Once the machine is fully defined and every geometrical parameter is obtained, different figures can be drawn before calculating any operating results. This feature helps the designer to overview the arrangement to be calculated and ensure there are no errors in the geometry. The views that are given are the following: the frontal section of the machine (**Figure 24**), the transversal section of the machine (**Figure 24**), the detail of the stator slot (**Figure 24**), the detail of the rotor pole and winding (**Figure 25**) and the detail of the end winding of the rotor (**Figure 25**). The obtained figures for the analysed motor are shown below.

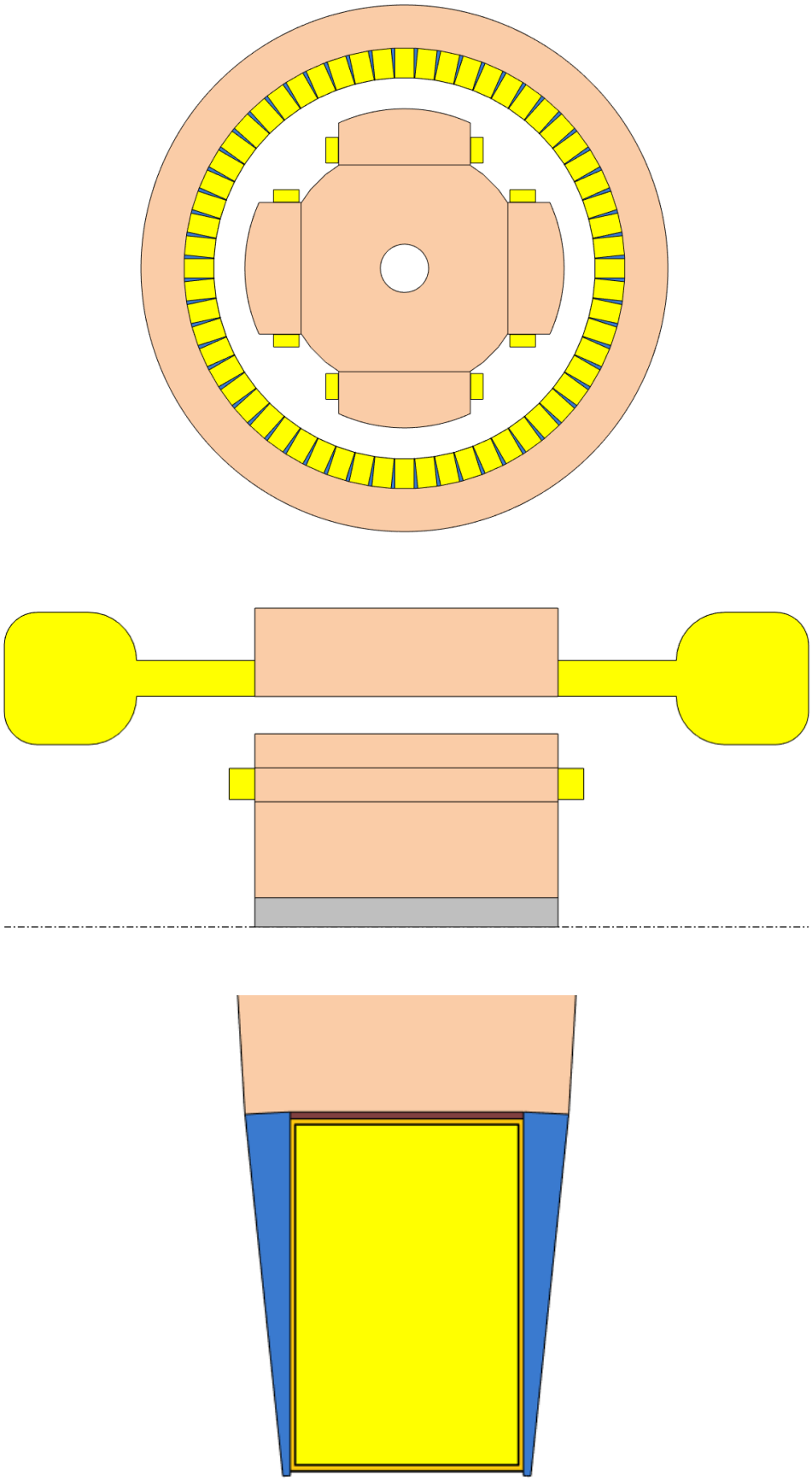

Figure 24. Frontal section (up), transversal section (centre) and stator slot (bottom) of the machine

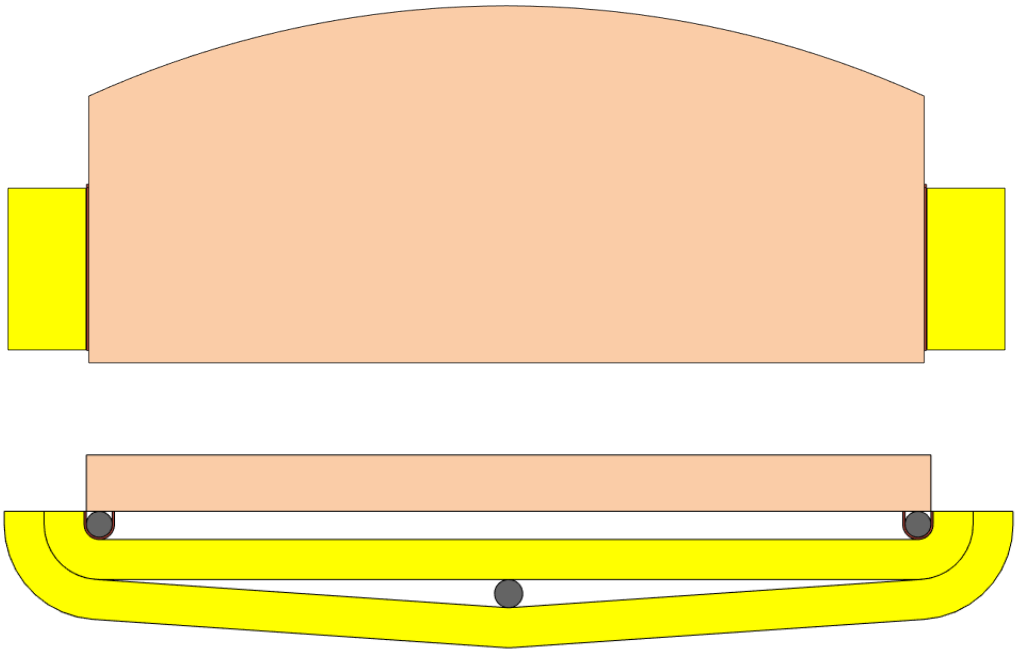

Figure 25. Detail of the rotor pole and winding (up) and the rotor end winding (bottom).

3.2.1.4. FEMM® Configuration

On this section, the configuration parameters for the FEMM® evaluation are calculated. With the input values of the output power, the rated voltage, the number of phases, the power factor and an estimation of the motor electromagnetic efficiency, a reference current (I_{ref}) is calculated. Depending on the control used for the machine (MTPA or I_q), the following configuration parameters are described:

- I_{min}. Defined as zero.
- I_{max}. Double of the reference current.
- ψ_{min}. Depending on the control type.
- ψ_{max}. Depending on the control type.
- Current matrix size. Defined as three.
- ψ matrix size. Depending on the control type.
- Number of simulations. Defined as two. The higher the number, the more accurate the solution.

In order to later obtain the rated current, two matrixes will be generated: one containing an interpolation between I_{min} and I_{max} and the other one containing an interpolation between ψ_{min} and ψ_{max}.

3.2.1.5. Calculation

The whole calculation stage can be divided in several steps, as was shown in **Figure 22**. In the first four phases, the temperature, frequency and geometrical dependant parameters are calculated as well as the electric resistances and the inductances. Then, the point of operation is calculated with the FEMM method and, finally, the resulting magnetic and electric parameters are calculated along with the losses and efficiencies.

The temperature dependant parameter that is determined is the conductivity of the winding at the supposed working temperature in the 'input data' ($\sigma_{w,hot}$). With that working temperature (T_w), the reference conductivity of the material ($\sigma_{w,cold}$), the reference winding temperature ($T_{ref,w}$) and the temperature coefficient ($k_{\rho,T}$) defined in the material section, the resulting conductivity can be easily determined (1).

$$\sigma_{w,hot} = \frac{\sigma_{w,cold}}{\left[1 + k_{\rho,T} \cdot \left(T_w - T_{ref,w}\right)\right]} \quad (1)$$

The frequency of the machine determines some parameters of the calculated motor. First, the BH curve of the stator and rotor lamination is dependant on the frequency. Therefore, to get the steel losses on the lamination, the BH curve has to be assessed. Also, the frequency affects the resistances and inductances of the machine, so a correction factor for those parameters is calculated.

On the other hand, the only geometrical parameter defined on this stage is the Carter factor of the machine, which depends on the Carter factor of the rotor and stator calculated previously (2). The Carter factor is related to the irregular distribution of the flux density on the airgap due to the slots.

$$k_C = k_{C,stator} \cdot k_{C,rotor} \quad (2)$$

The winding resistance per phase of the rotor ($R_{ph,hot,r,DC}$) is calculated with the copper phase length ($l_{Cu,ph}$), the material conductivity ($\sigma_{w,hot}$), the conductor section (S_{Cu}) and the number of parallel coils ($N_{w,par}$), as it conducts a DC current (3). However, for the stator winding resistance, a previously calculated correction factor (KR_s) should be applied to the correspondent DC resistance to obtain the AC resistance of the coils (4).

$$R_{ph,hot,r,DC} = \frac{l_{Cu,ph,r}}{\sigma_{w,hot,r} \cdot S_{Cu,r} \cdot N_{w,par,r}^2} \quad (3)$$

$$R_{ph,hot,s,AC} = KR_s \cdot \frac{l_{Cu,ph,s}}{\sigma_{w,hot,s} \cdot S_{Cu,s} \cdot N_{w,par,s}^2} \quad (4)$$

Even if the inductances will be determined more precisely during the FEMM® calculation, a first approximation is deduced on this section. As with the resistances, first the DC inductances are calculated and then, applying a frequency correction factor, the AC inductances are determined. Several inductance parameters are calculated. First, the differentiated 'd' and 'q' armature inductances and then the dispersion DC inductances are obtained. Again, with the DC values and the frequency correction factor, the AC inductances are assessed.

Once every aforementioned parameter is defined, it begins the FEMM® calculation (**Figure 26**). FEMM® is a multi-static method; therefore, it calculates one solution at once with specific conditions, it does not calculate a transient solution. First of all, the stator and rotor geometries are defined in FEMM®, according to the periodicity of the motor calculated on the dependant variables step. In the case of the example, the periodicity is four (5); therefore, only a quarter of the machine is evaluated to obtain a full solution. In this stage the materials are also defined for each region along with the mesh quality (**Figure 27**).

$$Machine\ periodicity = GCD(poles, slots) \quad (5)$$

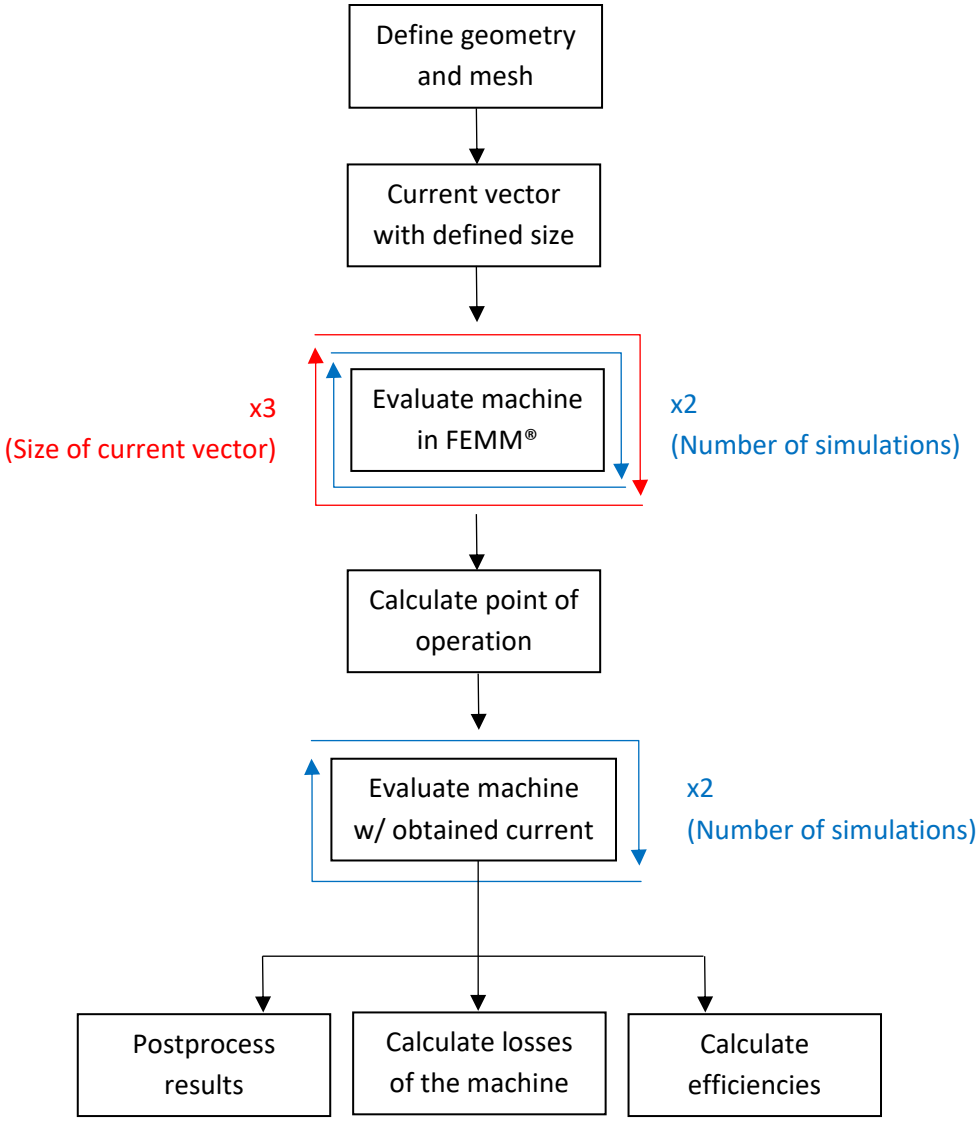

Figure 26. FEMM calculation structure.

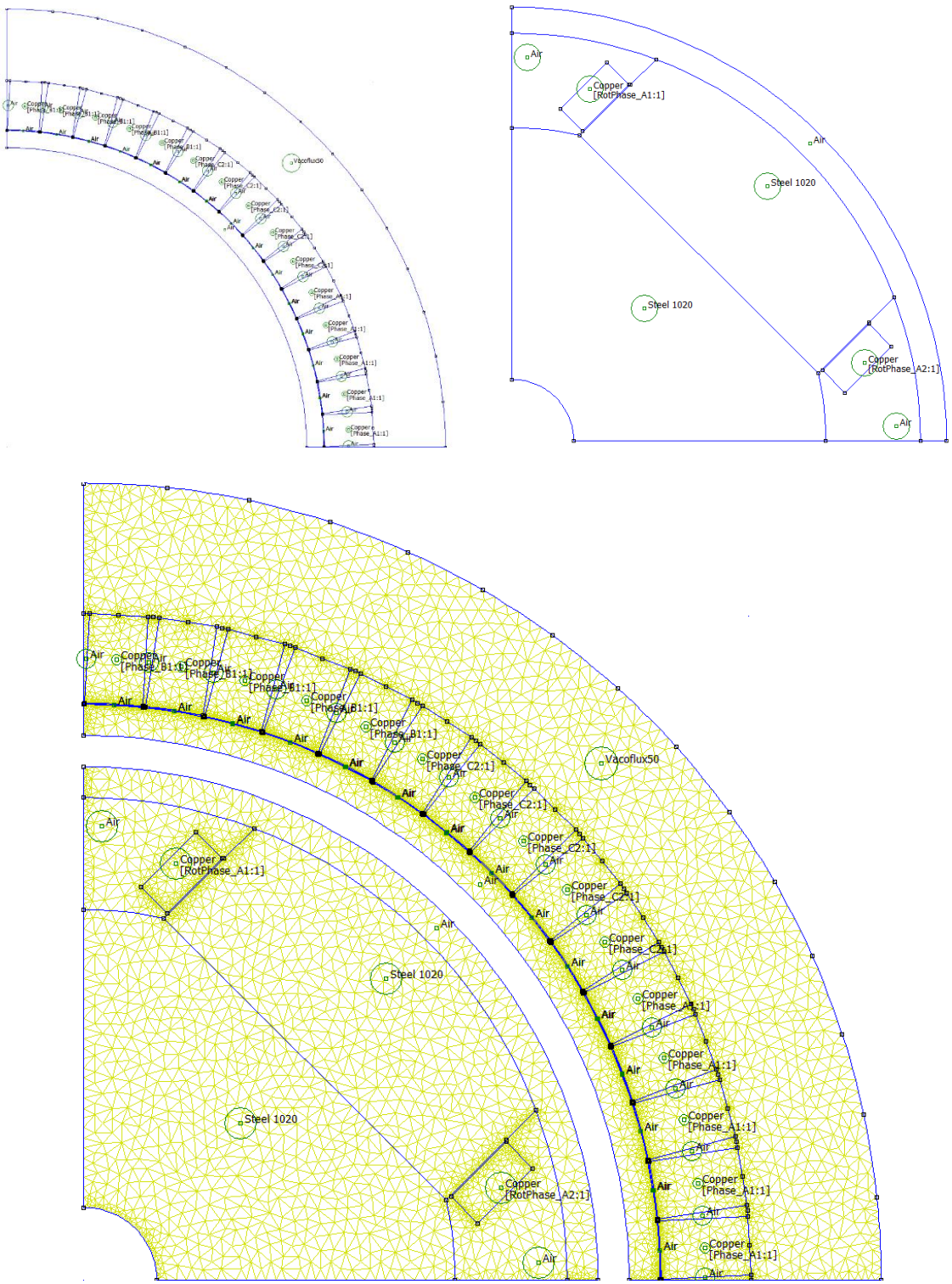

Figure 27. Geometric FEMM definition of the stator (up, left), the rotor (up, right) and the machine mesh (bottom).

Later on, the aforementioned matrixes (in **3.2.1.4**) are described, evaluating the problem for three different conditions (as the current matrix size defined in the FEMM® configuration was three). For each of the three evaluations the machine is simulated the number of times specified also in the FEMM® configuration phase (in this case, the number of simulations was two). As a result, the parameter matrixes contain three-sized vectors (one for each condition) with several

electromagnetic parameters such as the phase current, the flux densities on the airgap and the yokes, the flux linkage on load of the machine or the back EMF.

In order to obtain the point of operation, the three-sized vector are interpolated to determine a bigger size vector (in this case of 257 values) to achieve more accurate results. With the 'd' and 'q' current matrixes and the 'd' and 'q' flux linkage matrixes, the corresponding line voltage matrix (6), the power factor matrix, the electromagnetic torque (7) and power (8) matrixes, the loss matrix, and, finally, the output power matrix (9) are obtained.

$$U_{ph,s} = \sqrt{0.5 \cdot \left[\left(R_{ph,hot,s} \cdot I_d - \omega_e \cdot \lambda_q\right)^2 + \left(R_{ph,hot,s} \cdot I_q + \omega_e \cdot \lambda_d\right)^2\right]} \quad (6)$$

$$\tau_{em} = \frac{m_s \cdot p_p}{2} \cdot \left(\lambda_d \cdot I_q - \lambda_q \cdot I_d\right) \quad (7)$$

$$P_{em} = \tau_{em} \cdot \omega_m \quad (8)$$

$$P_{out} = P_{em} - P_{loss} \quad (9)$$

Then, with the output power predefined as input data, the point of operation is found within the output power 257-sized matrix. At last, according to the position where the output power was found, the current and ψ values can be defined on the same corresponding matrix position (**Figure 32**).

$$\begin{pmatrix} (P_{out})_1 \\ \vdots \\ \boxed{(P_{out})_n} \\ \vdots \\ (P_{out})_{257} \end{pmatrix} \rightarrow \begin{pmatrix} I_{min} \\ \vdots \\ \boxed{I_n} \\ \vdots \\ 2 \cdot I_{max} \end{pmatrix}$$

Figure 28. Obtention of the operating point current.

After the point of operation is determined with the obtained current and ψ values, the machine is evaluated once again with the FEMM® tool. When the solution is calculated and all the parameters are postprocessed, the electric ($P_{Cu,r}$, $P_{Cu,s}$) (10), magnetic ($P_{Fe,r}$, $P_{Fe,s}$) and mechanic losses (P_{mec}) are determined, along with the machine efficiencies.

$$P_{Cu} = m_s \cdot R_{ph,hot} \cdot I_{ph}^2 \quad (10)$$

The losses in the rotor are far smaller than in the stator for two main reasons. First, as the rotor winding is superconductor, the losses in the copper due to the Joule effect are neglectable. On the other hand, the flux density in the rotor steel is constant (not as in the stator); therefore, the losses due to the hysteresis and Eddy currents are also virtually zero. The stator losses depend on the stator current and the winding resistance and on the saturation of the steel.

Finally, the machine electromagnetic efficiency can be calculated as the quotient between the output and the input power.

3.2.1.6. Machine results

The obtained results of the calculation can be shown both graphically and numerically. The graphic results are obtained in the FEMM® tool. The flux density colour map is particularly interesting due to the fast overview of the magnetic field value all along the machine. An example of that result is shown in the following figure (**Figure 29**):

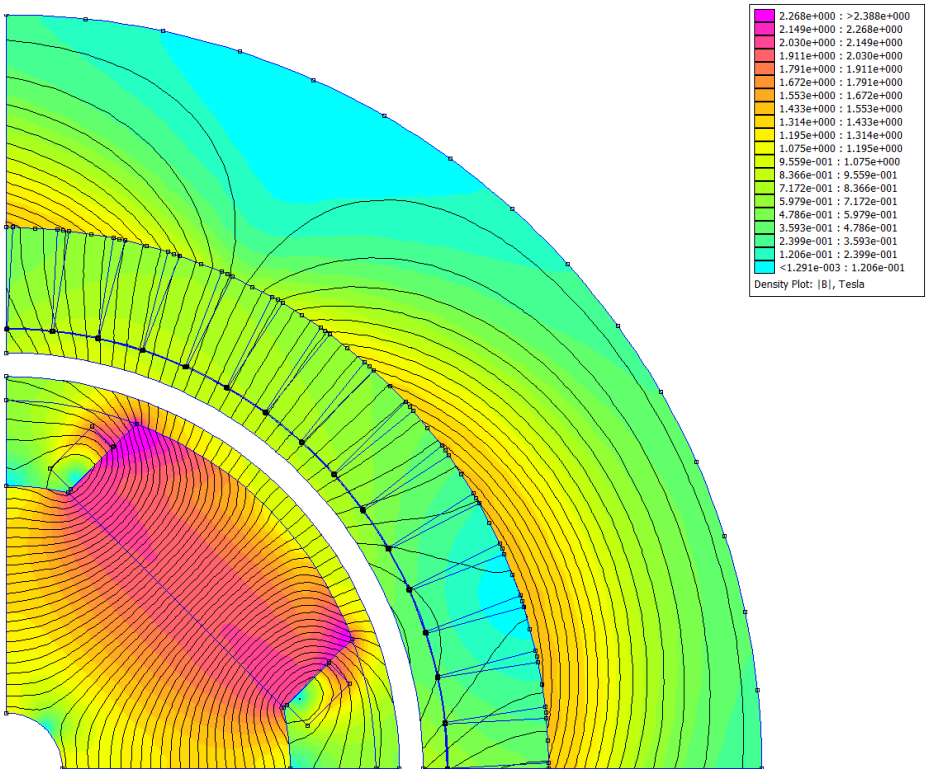

Figure 29. Map colour of the flux density in the motor.

Apart from the flux density map, the field density and current density map can also be seen in FEMM. Moreover, specific values for the aforementioned parameters are shown by clicking a particular point in the motor.

On the other hand, more diverse numerical results are obtained in the IPED®. Every previously described parameter is saved on a structure in Matlab, called `struct_machine`. This structure is divided in the following ten fields:

- `algortm`
- `e_magnetic`
- `geo_rotor`
- `winding`
- `geo_stator`
- `thermal`
- `project`
- `geo_mechanic`
- `materials`
- `postpro`

Nevertheless, for this project, the most useful fields are the `e_magnetic`, `geo_rotor`, `geo_stator`, `winding` and `materials`. On the `e_magnetic` field, the electromagnetic parameters are saved. On the `geo_rotor`, `geo_stator` and `winding` fields, every geometric parameter related to the rotor, the stator and the winding respectively are written. Finally, all the information regarding the lamination, winding, cooling and insulating materials are saved on the `materials` field.

In order to validate the developed HTS motor design module, it has been compared with Ansys MotorCAD® [85], another motor design software. In the next figures, the geometry (**Figure 30**) and simulation results (**Figure 31** and **Table 10**) of both programs are shown.

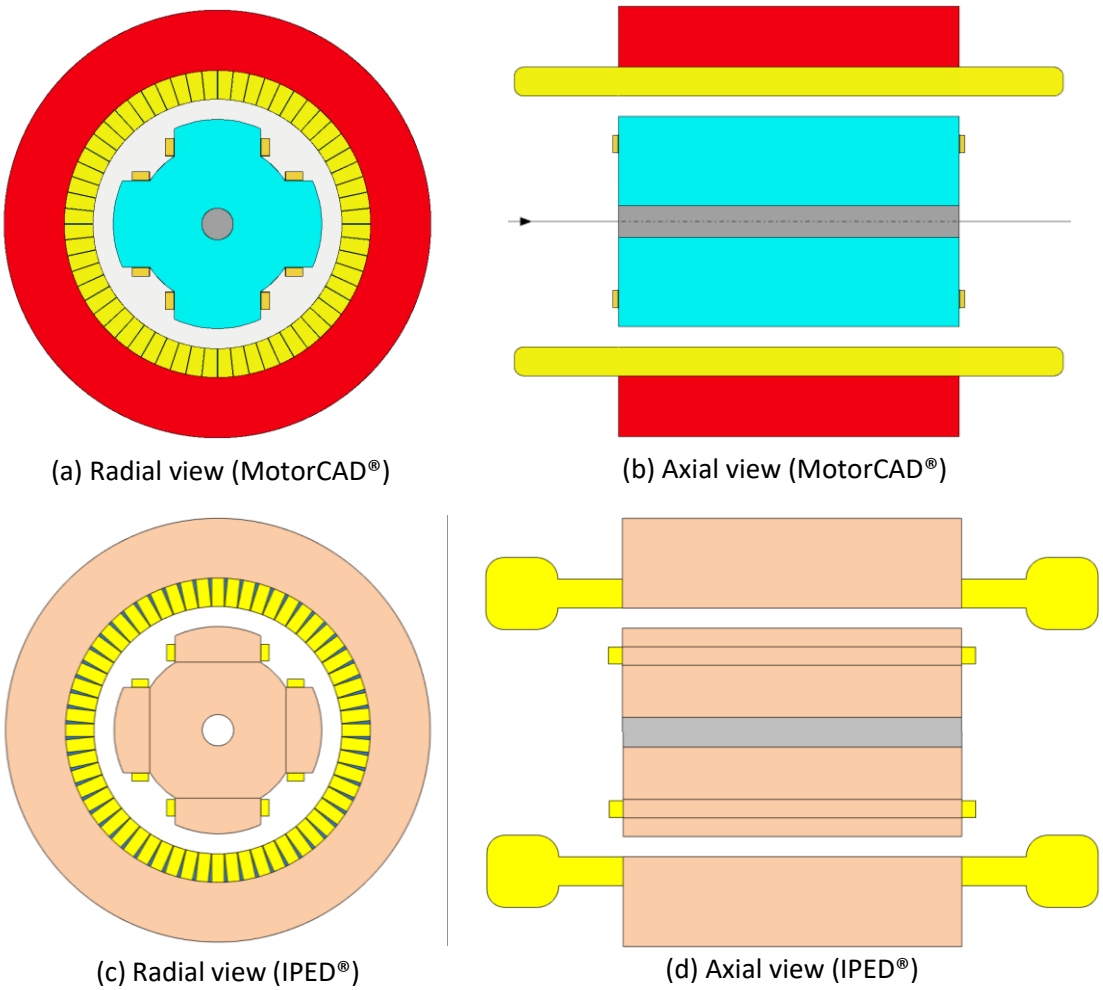

(a) Radial view (MotorCAD®) (b) Axial view (MotorCAD®)

(c) Radial view (IPED®) (d) Axial view (IPED®)

Figure 30. Different views of the motor on MotorCAD® and IPED® software.

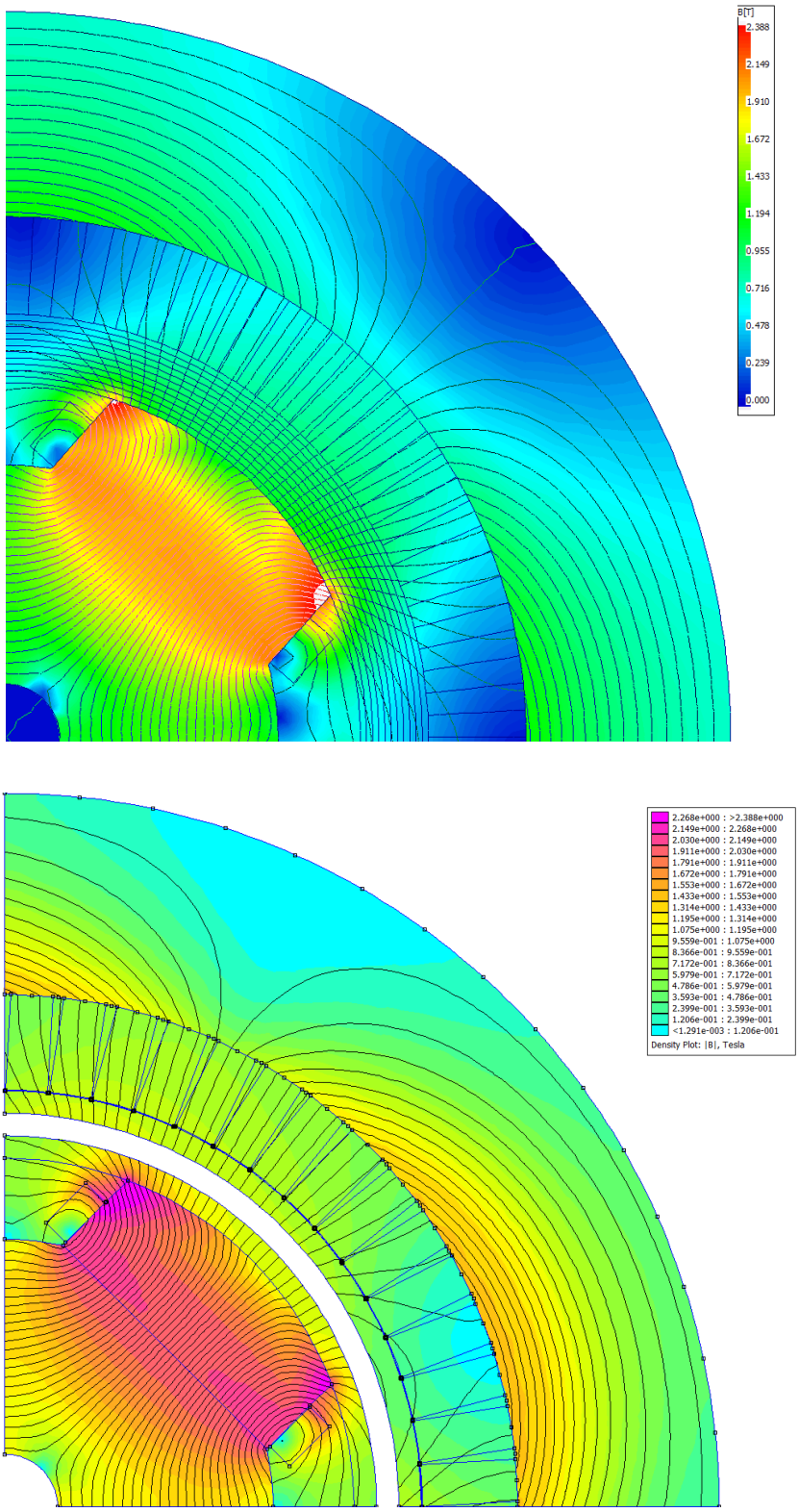

Figure 31. Flux density results on MotorCAD® (up) and IPED® (down).

Table 10

Summary of the motor power parameters (1st design).

	Parameter	Value MotorCAD®	Value IPED®	Units
Power parameters	Output power	2.001	2.006	MW
	Efficiency	99.54	98.61	%
	VDC	1200	1200	V
	I_{PH}	1560	1588	A
	PF	0.988	0.986	-
	m	1837	1836	kg
	Power density	1.09	1.09	kW/kg

3.2.2. Conclusions

As has been presented in **Figure 30**, **Figure 31** and **Table 10**, the obtained results with the IPED® tool and with Ansys MotorCAD® are practically identical. Even in the parameters where the error is the greatest (less than a 1% in the case of the efficiency), the matter of the error is known and justified (differences on the calculation procedures, for example). Therefore, it can be concluded that the developed IPED® HTS module is clearly valid and as accurate as the commercial electric machine designing program Ansys MotorCAD®.

Chapter 4

Predesign

4.1. First Proposed Design

On this chapter the proposed superconducting motor predesign will be described. As it has been explained, this thesis is framed on the HIVOMOT European project. The geometrical and power requirements chosen for the project in **2.6** are listed on the **Table 11**.

Table 11

Summary of the requirements of the HIVOMOT project.

Parameter	Value	Units
Output power	2	MW
Rotational speed	2700	RPM
Efficiency	>95	%
Power density	>7.7	kW/kg
VDC	3000	V
Switching frequency	30	kHz
Fan diameter	3	m
Spinner diameter	0.6-0.9	m
Nacelle length	1	m
Superconducting part	DC Field Winding	-
Superconducting material	2G HTS, MgB2	-

The design of the rotor and its winding was carried out by Suprasys and the geometrical parameters defined for the first predesign are as follows on **Table 12**.

Table 12

Summary of the rotor parameters.

	Parameter	Value	Units
Rotor	Poles	4	-
	Pole Width	150	mm
	Pole Depth	32	mm
	Pole Tip Depth	32	mm
	Pole Surface Radius	181.75	mm
	Airgap	35	mm
	I_{POL}	59000	A
	Rotor Slot Width	14.8	mm
	Rotor Slot Depth	29.5	mm
	Winding Turns	1	-
	Shaft Diameter	55	mm
	Lamination material	Steel 1020	-
Stator	Slots	60	-
	Stator Exterior Diameter	743.5	mm
	Stator Interior Diameter	433.5	mm
	Slot Depth	50	mm
	Stack Length	587.5	mm

The full radial and axial geometry is shown on the following figure (**Figure 32**).

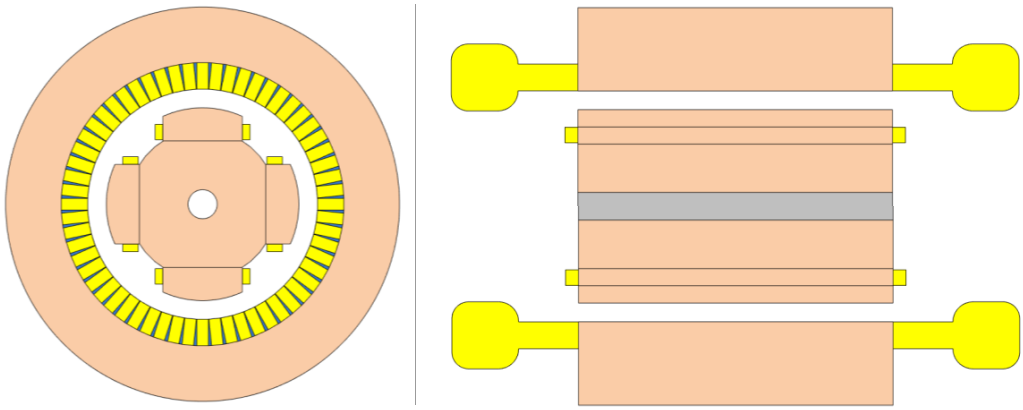

(c) Radial view (d) Axial view

Figure 32. Different views of the motor on the IPED® software.

A first simulation was carried out with these parameters and the results can be seen below (**Figure 33**). **Table 13** summarizes the motor performance under load conditions.

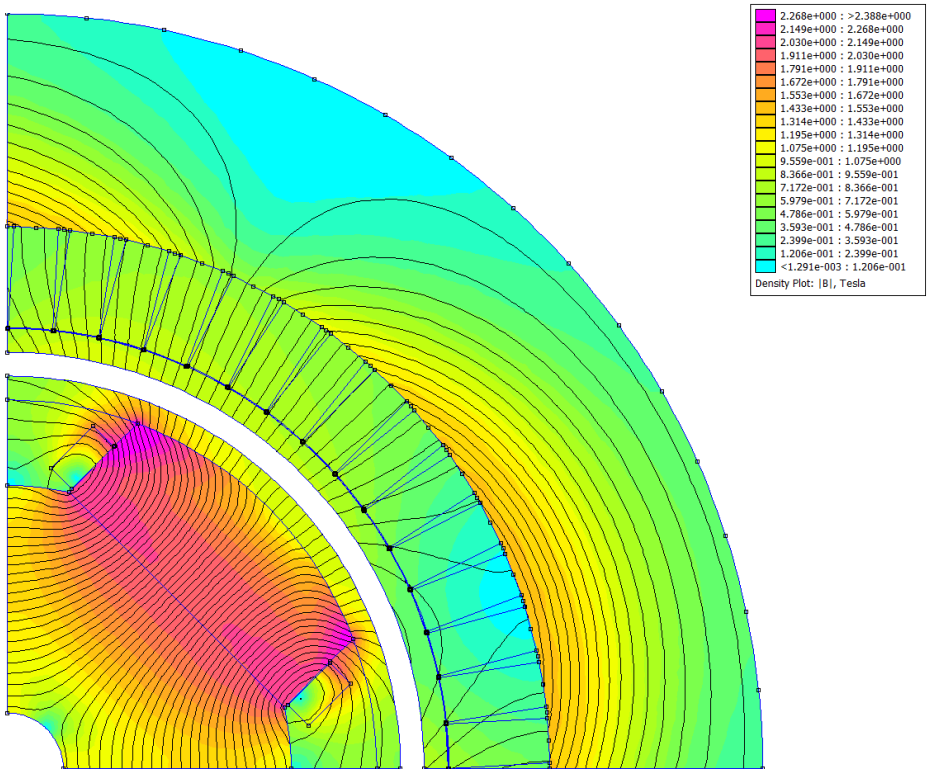

Figure 33. Flux density results on IPED®.

Table 13

Summary of the motor power parameters (1st design).

	Parameter	Value	Units
Power parameters	Output power	2.006	MW
	Efficiency	98.61	%
	VDC	1200	V
	I_{PH}	1588	A
	PF	0.986	-
	m	1836	kg
	Power density	1.09	kW/kg

As can be seen on the **Table 13**, the total mass of the motor is oversized, giving a power density of 1.09 kW/kg, far away from the expected 7.7 kW/kg.

4.2. Optimization of the Stator

Three principal parameters are potentially optimizable: the stack length, the size of the stator yoke and the slot size:

- In order to reduce the length of the motor, the stator phase current is increased from the initial 1560 A to 2800 A, when the resulting winding temperature reaches 180 ºC (set as temperature limit for the conductor). This leads to a higher output power; therefore, the proposed output power of 2 MW can be reached reducing the stack length of the motor from 587.5 to 327.5 mm.
- Secondly, the stator yoke is reduced as the flux density is relatively low. As the material used on the stator lamination (Vacoflux50) allows flux densities of 2.1-2.2 T, the stator external diameter is decreased from the initial 743.5 mm to 625 mm, before the saturation of the steel becomes influential.
- Finally, the stator slot is adjusted to the size of the conductor. The stator winding consists on a unique-turn rectangular cupper conductor of a cross section of 21x32 mm, area chosen according to the current density of the conductor. Consequently, the slot depth can be decreased from the initial 50 mm to 34 mm. Due to this reduction, the external diameter of the stator changes from the aforementioned 625 mm to 600 mm. Again, with these parameters the output power is increased, allowing a new stack length shortening from the previous 327.5 mm to 286 mm.

The new model geometry is shown in **Figure 34**.

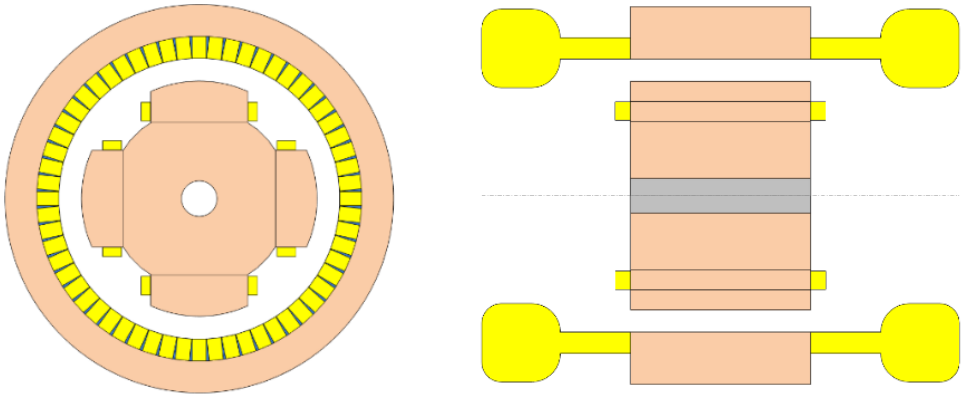

Figure 34. Different views of the optimized motor on IPED®.

The output power parameters are described in **Table 14** and the flux density is shown in **Figure 35**.

Table 14

Summary of the motor power parameters (2nd design).

	Parameter	Value	Units
Power parameters	Output power	2.006	MW
	Efficiency	96.87	%
	I_{PH}	2818	A
	PF	0.948	-
	m	741	kg
	Power density	2.71	kW/kg
Stator	Slots	60	-
	Stator Exterior Diameter	600	mm
	Slot Depth	34	mm
	Stator Coil Width	21	mm
	Stator Coil Depth	32	mm
	Winding Turns	1	-
	Stack Length	286	mm

On the **Table 15** a breakdown of the motor mass is exposed. Even if the total mass has been optimized from 1840 to 720 kg, the power density of the motor is still poor with a value of 2.8 kW/kg. Nevertheless, with future optimizations the aim value of 7.7 kW/kg should be surpassed.

Table 15

Mass breakdown of the motor (2nd design).

	Stator Lam (kg)	Stator Wind (kg)	Rotor Lam (kg)	Rotor Wind (kg)	**Total Mass**
Value	191.9	349.3	186.0	13.6	**741**

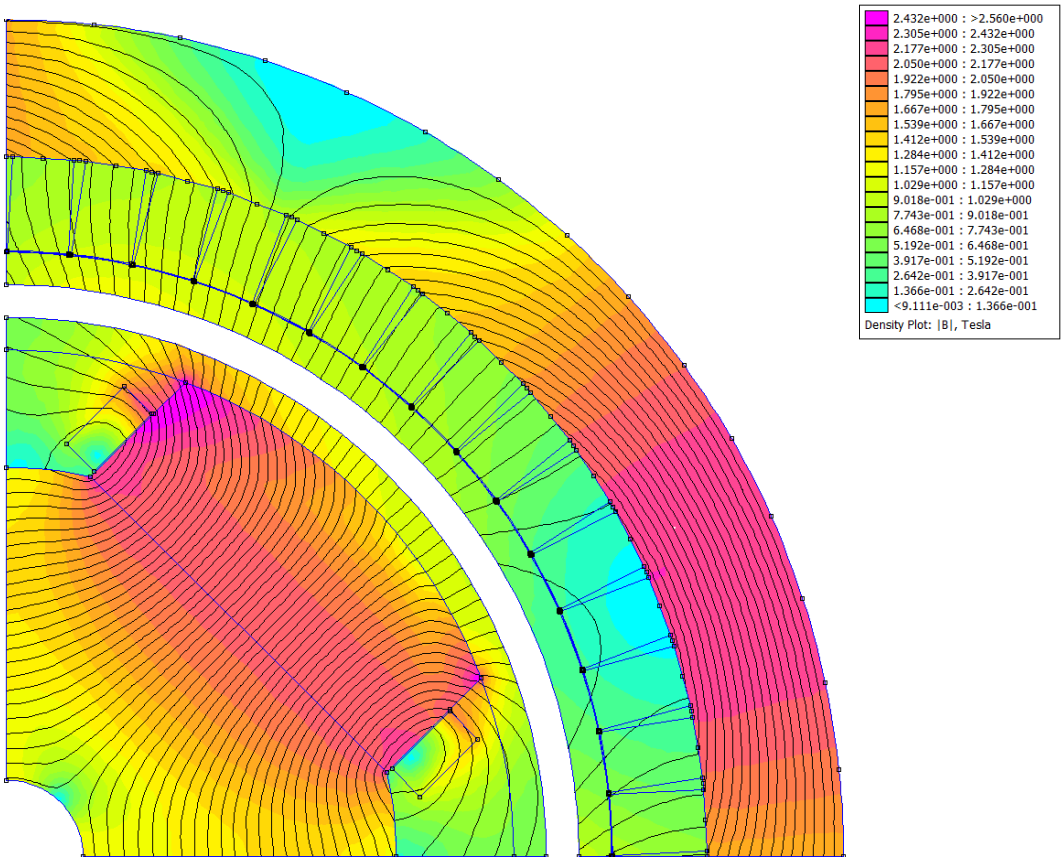

Figure 35. Flux density results on IPED®.

Chapter 5

Conclusions and future work

5.1. Conclusions

The previous chapters have covered the main aspects of the state of the art in High Temperature Superconductors for aircraft propulsion along with the description of the HTS electric motor design module developed. A general overview on the history of the electric aircraft and future studies has been given. Different groundbreaking technologies such as the distributed propulsion, the Boundary Layer Ingestion or the High Temperature Superconductors have been discussed with an emphasis on the last one. As a conclusion for the state of the art, some power and design requirements have been defined for a High Temperature Superconducting motor.

Afterwards, a HTS motor calculation module has been developed on IPED® and it has been validated by the comparison with the commercial program, Ansys MotorCAD. The results obtained from this assessed were considerably accurate; therefore, the module was regarded as valid.

Later, a predesign of a HTS motor has been presented and assessed. The topology consisting of a superconducting rotor and a conventional stator has emerged as one of the most promising candidates in terms of overall system efficiency. Furthermore, the optimum superconducting material for the envisaged approach is the MgB_2 compound. For this reason, it has been decided to orient the present project towards this design. The requirements of this architecture have been reviewed as well as the main disadvantages.

Finally, a first design with a superconducting rotor configuration suggested by Suprasys has been proposed. Although the power densities achieved in the pre-design are far from the target, the design is expected to be optimised in the coming months, lowering the total mass and giving the same output power.

5.2. Future work

As it was mentioned in **4.2**, the target power density of 7.7 kW/kg has not been achieved with the proposed motor predesign. In order to accomplish the objective, a redesign should be done in several aspects such as the number of poles of the rotor, an alternative superconducting material, a variation on the rotor geometry, the stator winding or the current density of the non-superconducting coils.

Along with the previously mentioned minimum power density aim, the following objectives should be completed during the HIVOMOT project:

- Investigation on modelling of high voltage electrical systems at high altitude for fundamental understanding of the technical issues related to inverter-fed HV insulation and arcing effects in electrical machines.
- Research into insulation approaches and assessment of their reliability and safety at high altitude.
- Electromagnetic, electrical, thermal and mechanical design of actual topologies of electrical machines in order to evaluate technology limits for high power and high voltage operation in A/C applications.
- Comparison of available and foreseen HTS materials for their use in electric machines for high volumetric and mass power density.
- Investigation on thermal management systems for cryo-cooled HTS windings for electric machines in aircraft environment.
- Analysis of manufacturing processes to achieve the required HTS coils geometry, provide the winding voltage to the conductor in order to avoid quenches and optimize the winding volume.
- Full design of a MW-class HTS electric motor concept and development of a lab-scale validator, applying the most suitable techniques investigated during the project for HV and high-altitude operation, including the thermal management.

Bibliography

[1] B. J. Brelje and J. R. R. A. Martins, “Electric, hybrid, and turboelectric fixed-wing aircraft: A review of concepts, models, and design approaches,” *Prog. Aerosp. Sci.*, vol. 104, no. June 2018, pp. 1–19, 2019.

[2] “Ceit BRTA,” 2021. [Online]. Available: https://www.ceit.es/.

[3] “SUPRASYS SL,” 2021. [Online]. Available: https://suprasys.es/es/.

[4] “Antec Magnets SLU,” 2021. [Online]. Available: https://antec-group.com/.

[5] “Alconza Berango SL,” 2021. [Online]. Available: https://www.alconza.com/es/.

[6] “Sector by sector: where do global greenhouse gas emissions come from? - Our World in Data.” [Online]. Available: https://ourworldindata.org/ghg-emissions-by-sector. [Accessed: 09-Apr-2021].

[7] H. Gesell, F. Wolters, and M. Plohr, “System analysis of turbo electric and hybrid electric propulsion systems on a regional aircraft,” *31st Congr. Int. Counc. Aeronaut. Sci. ICAS 2018*, no. December, 2018.

[8] F. Berg, J. Palmer, P. Miller, M. Husband, and G. Dodds, “HTS electrical system for a distributed propulsion aircraft,” *IEEE Trans. Appl. Supercond.*, vol. 25, no. 3, 2015.

[9] A. S. Gohardani, G. Doulgeris, and R. Singh, “Challenges of future aircraft propulsion: A review of distributed propulsion technology and its potential application for the all electric commercial aircraft,” *Prog. Aerosp. Sci.*, vol. 47, no. 5, pp. 369–391, 2011.

[10] H. D. Kim, “Distributed propulsion vehicles,” *27th Congr. Int. Counc. Aeronaut. Sci. 2010, ICAS 2010*, vol. 1, pp. 55–65, 2010.

[11] “The Tissandier ‘La France’ airship, 1883. | Science Museum Group Collection.” [Online]. Available: https://collection.sciencemuseumgroup.org.uk/objects/co29480/the-tissandier-la-france-airship-1883-aircraft-airships. [Accessed: 29-Mar-2021].

[12] L. A. Costello and L. A. Costello, “State of the Art of Piloted Electric Airplanes , NASA ’ s Centennial Challenge Data and Fundamental Design Implications by,” 2011.

[13] “Technical Data - Lange Aviation. Antares 20E,” 2003. [Online]. Available: https://www.lange-aviation.com/en/produkte/antares-20e/techn-daten/. [Accessed: 25-Mar-2021].

[14] “ElectraFlyer.com - The World Famous ElectraFlyer-C,” 2008. [Online]. Available: https://www.electraflyer.com/electraflyerc.php. [Accessed: 25-Mar-2021].

[15] “Yuneec,” 2009. [Online]. Available: https://www.yuneec.com/es_ES/home.html. [Accessed: 25-Mar-2021].

[16] “Pipistrel Taurus Electro G2,” 2011.

[17] "Alpha Electro – Pipistrel Aircraft," 2015. [Online]. Available: https://www.pipistrel-aircraft.com/aircraft/electric-flight/alpha-electro/. [Accessed: 25-Mar-2021].

[18] "Diamond Aircraft proudly presents the world's first serial hybrid electric aircraft 'DA36 E-Star' - Diamond Aircraft Industries," 2011. [Online]. Available: https://www.diamondaircraft.com/en/about-diamond/newsroom/news/article/diamond-aircraft-proudly-presents-the-worlds-first-serial-hybrid-electric-aircraft-da36-e-star/. [Accessed: 25-Mar-2021].

[19] "Long-ESA – Flight of the Century | Flight of the Century," 2012. [Online]. Available: http://www.flightofthecentury.com/long-esa/. [Accessed: 25-Mar-2021].

[20] N. Lapeña-Rey, J. Mosquera, E. Bataller, and F. Ortí, "First Fuel-Cell Manned Aircraft," 2008.

[21] "e-Genius | Institute of Aircraft Design | University of Stuttgart," 2011. [Online]. Available: https://www.ifb.uni-stuttgart.de/en/research/aircraftdesign/mannedaircraft/e-genius/. [Accessed: 25-Mar-2021].

[22] "Electric flight - Zero emission - Airbus," 2016. [Online]. Available: https://www.airbus.com/innovation/zero-emission/electric-flight.html#projects. [Accessed: 25-Mar-2021].

[23] Airbus, "Airbus, 'E-Fan project.,'" 2020. [Online]. Available: https://www.airbus.com/innovation/zero-emission/electric-flight/e-fan-x.html.

[24] "Rolls-Royce and Airbus cancel E-Fan X project | The Engineer The Engineer," 2020. [Online]. Available: https://www.theengineer.co.uk/e-fan-x-project-cancelled/. [Accessed: 30-Mar-2021].

[25] "CityAirbus - Urban Air Mobility - Airbus," 2019. [Online]. Available: https://www.airbus.com/innovation/zero-emission/urban-air-mobility/cityairbus.html. [Accessed: 30-Mar-2021].

[26] "Extra 330LE Electric Aircraft - Aerospace Technology," 2017. [Online]. Available: https://www.aerospace-technology.com/projects/extra-330le-electric-aircraft/. [Accessed: 25-Mar-2021].

[27] "Ampaire EEL," 2021. [Online]. Available: https://www.ampaire.com/vehicles/electric-eel-aircraft. [Accessed: 26-Mar-2021].

[28] "Cessna eCaravan becomes largest electric aircraft to fly," 2020. [Online]. Available: https://www.aerotime.aero/25091-cessna-ecaravan-magnix-first-flight. [Accessed: 30-Mar-2021].

[29] "Seaplane to ePlane: Flight Test Confirmed – Harbour Air: North America's Largest Seaplane Airline – Since 1982," 2019. [Online]. Available: https://www.harbourair.com/seaplane-to-eplane-flight-test-confirmed/. [Accessed: 26-Mar-2021].

[30] T. -Plevnik *et al.*, "Pipistrel Taurus G4: on Creation and Evolution of the Winning Aeroplane of NASA Green Flight Challenge 2011," *Strojniški vestnik-Journal Mech. Eng.*, vol. 57, pp. 869–878, 2011.

[31] "NASA - The EcoEagle," 2011.

[32] "ElectraFlyer.com - The World Famous ElectraFlyer-ULS," 2012. [Online]. Available: https://www.electraflyer.com/electraflyer-uls.php. [Accessed: 25-Mar-2021].

[33] "Electric propulsion components with high power densities for aviation," 2015.

[34] "Watts up - aeroplanes go hybrid-electric | University of Cambridge," 2014. [Online]. Available: https://www.cam.ac.uk/research/news/watts-up-aeroplanes-go-hybrid-electric. [Accessed: 25-Mar-2021].

[35] "Spirit of innovation – Rolls-Royce," 2021. [Online]. Available: https://careers.rolls-royce.com/india/stem/spirit-of-innovation. [Accessed: 26-Mar-2021].

[36] "X-57 Maxwell," 2021. [Online]. Available: https://www.nasa.gov/specials/X57/. [Accessed: 26-Mar-2021].

[37] "The Future of Aircraft Propulsion is Electric | NASA." [Online]. Available: https://www.nasa.gov/centers/armstrong/Features/leaptech.html. [Accessed: 31-Mar-2021].

[38] "AIRCRAFT | Eviation," 2021. [Online]. Available: https://www.eviation.co/aircraft/. [Accessed: 26-Mar-2021].

[39] A. P. Plas *et al.*, "Performance of a Boundary Layer Ingesting (BLI) Propulsion System AIAA 2007-450."

[40] A. Uranga *et al.*, "Boundary Layer Ingestion Benefit of the D8 Transport Aircraft," *3693 AIAA J.*, vol. 55, no. 11, 2017.

[41] "Ampaire Tailwind," 2021. [Online]. Available: https://www.ampaire.com/vehicles/tailwind™-aircraft. [Accessed: 26-Mar-2021].

[42] "STARC-ABL | SACD," 2021. [Online]. Available: https://sacd.larc.nasa.gov/asab/asab-projects-2/starc-abl/. [Accessed: 26-Mar-2021].

[43] "Airbus Voltair," 2021. [Online]. Available: https://www.vrpe.de/en/airbus-voltair/. [Accessed: 26-Mar-2021].

[44] "Airbus E-Thrust," 2021. [Online]. Available: https://www.vrpe.de/en/airbus-e-thrust/. [Accessed: 26-Mar-2021].

[45] J. L. Felder, "Fundamental Aeronautics Program Fixed Wing Project NASA N3-X with Turboelectric Distributed Propulsion," 2017.

[46] P. J. Masson, G. V. Brown, D. S. Soban, and C. A. Luongo, "HTS machines as enabling technology for all-electric airborne vehicles," *Supercond. Sci. Technol.*, vol. 20, no. 8, pp. 748–756, 2007.

[47] C. A. Luongo *et al.*, "Next generation more-electric aircraft: a potential application for hts superconductors," *IEEE Trans. Appl. Supercond.*, vol. 19, no. 3, pp. 1055–1068, 2009.

[48] "Eco Otter SX," 2021. [Online]. Available: https://www.ampaire.com/vehicles/eco-otter-sx-aircraft. [Accessed: 26-Mar-2021].

[49] "Zunum Aero," 2021. [Online]. Available: https://zunum.aero/. [Accessed: 26-Mar-2021].

[50] "XTI Aircraft - the TriFan 600," 2021. [Online]. Available: https://www.xtiaircraft.com/xti-triFan-600#Technology-Reimagined. [Accessed: 26-Mar-2021].

[51] "Boeing: How sweet the future of aviation," 2021. [Online]. Available: https://www.boeing.com/features/innovation-quarterly/aug2017/feature-technical-sugar.page. [Accessed:

26-Mar-2021].

[52] "Ce-Liner: Bauhaus Luftfahrt," 2021. [Online]. Available: https://www.bauhaus-luftfahrt.net/en/topthema/ce-liner/. [Accessed: 26-Mar-2021].

[53] B. T. Schiltgen, J. L. Freeman, and D. W. Hall, "Aeropropulsive Interaction and Thermal System Integration within the ECO-150: A Turboelectric Distributed Propulsion Airliner with Conventional Electric Machines," vol. 94404, 2016.

[54] L. Lusuardi and A. Cavallini, "The Problem of Altitude When Qualifying the Insulating System of Actuators for More Electrical Aircraft," *2018 IEEE Int. Conf. Electr. Syst. Aircraft, Railw. Sh. Propuls. Road Veh. Int. Transp. Electrif. Conf. ESARS-ITEC 2018*, pp. 0–3, 2019.

[55] L. Lusuardi, A. Cavallini, P. Mancinelli, G. De La Calle Manuel, J. M. Martinez-Tarifa, and G. Robles, "Design criteria for inverter-fed Type 1 motors," *Proc. 2016 IEEE Int. Conf. Dielectr. ICD 2016*, vol. 2, pp. 605–608, 2016.

[56] N. Hayakawa, Y. Daicho, T. Kaji, and H. Kojima, "Estimation of Partial Discharge Inception Voltage under Repetitive Inverter Surge Voltage by Volume-Time Theory," *Annu. Rep. - Conf. Electr. Insul. Dielectr. Phenomena, CEIDP*, vol. 2018-Octob, pp. 550–553, 2018.

[57] R. Shafaie and M. Kalantar, "Design of a 10-MW-class wind turbine HTS synchronous generator with optimized field winding," *IEEE Trans. Appl. Supercond.*, vol. 23, no. 4, 2013.

[58] G. Sarmiento *et al.*, "Design and Testing of Real Scale MgB 2 Coils for SUPRAPOWER 10 MW Wind Generators," no. October, pp. 1–7, 2015.

[59] T. Yanamoto, M. Izumi, K. Umemoto, T. Oryu, Y. Murase, and M. Kawamura, "Load Test of 3-MW HTS Motor for Ship Propulsion," *IEEE Trans. Appl. Supercond.*, vol. 27, no. 8, 2017.

[60] M. Zhang, F. Eastham, and W. Yuan, "Design and Modeling of 2G HTS Armature Winding for Electric Aircraft Propulsion Applications," *IEEE Trans. Appl. Supercond.*, vol. 26, no. 3, pp. 12–16, 2016.

[61] F. Weng, M. Zhang, T. Lan, Y. Wang, and W. Yuan, "Fully superconducting machine for electric aircraft propulsion: Study of AC loss for HTS stator," *arXiv*, 2019.

[62] R. M. Scanlan, A. P. Malozemoff, and D. C. Larbalestier, "Superconducting materials for large scale applications," *Proc. IEEE*, vol. 92, no. 10, pp. 1639–1654, 2004.

[63] Y. K. Kwon *et al.*, "Performance test of a 1 MW class HTS synchronous motor for industrial application," *Phys. C Supercond. its Appl.*, vol. 468, no. 15–20, pp. 2081–2086, Sep. 2008.

[64] V. Selvamanickam *et al.*, "Progress in performance improvement and new research areas for cost reduction of 2G HTS wires," *IEEE Trans. Appl. Supercond.*, vol. 21, no. 3 PART 3, pp. 3049–3054, 2011.

[65] V. L. Ginzburg, "Once again about high-temperature superconductivity," *Contemp. Phys.*, vol. 33, no. 1, pp. 15–23, 1992.

[66] A. Echarri and M. Spadoni, "Superconducting Nb3Sn: A review."

[67] C. Buzea and T. Yamashita, "Review of superconducting properties of MgB2," *Cond-Mat*, no. 1, pp. 1–35,

2001.

[68] A. Knizhnik, G. E. Shter, G. S. Grader, G. M. Reisner, and Y. Eckstein, “Interrelation of preparation conditions, morphology, chemical reactivity and homogeneity of ceramic YBCO,” *Phys. C Supercond. its Appl.*, vol. 400, no. 1–2, pp. 25–35, 2003.

[69] C. W. Chu, P. H. Hor, R. L. Meng, L. Gao, Z. J. Huang, and Y. Q. Wang, “Evidence for Superconductivity above 40 K in the La-Ba-Cu-0 Compound System,” 1987.

[70] M. S. Shalaby, H. M. Hashem, T. R. Hammad, L. A. Wahab, K. H. Marzouk, and S. Soltan, “Higher critical current density achieved in Bi-2223 High-T c superconductors,” 2016.

[71] C. W. Chu, “Superconductivity at Higher Temperatures in the Hg-Ba-Ca-Cu-O Compound System,” 1994.

[72] A. P. Drozdov, M. I. Eremets, I. A. Troyan, V. Ksenofontov, and S. I. Shylin, “Conventional superconductivity at 203 kelvin at high pressures in the sulfur hydride system.”

[73] Z. Yuheng, Z. Jianwu, T. Shun, and X. Gaojie, “34K superconductivity of bi2201 system,” *Phys. C Supercond. its Appl.*, vol. 341–348, pp. 643–644, 2000.

[74] Y. F. Yamada Yamashita, K. Wada, and K. Tachikawa, “STRUCTURE ANO SUPERCONOUCTING PROPERTIES OF Bi-2212 CYLINDERS PREPAREO BY DIFFUSION PROCESS ABSTRACT.”

[75] “ITP Aero,” 2021. [Online]. Available: https://www.itpaero.com/es/.

[76] M. K. Bradley, T. J. Allen, and C. K. Droney, “Subsonic Ultra Green Aircraft Research: Phase II – Volume II – Hybrid Electric Design Exploration,” *NASA Tech. Rep.*, vol. CR–2015-21, no. April, p. 76, 2015.

[77] F. Anton, S. Ag, C. Technology, T. Der Deutschen, and L.- Raumfahrtregionen, “eAircraft: Hybrid-elektrische Antriebe für Luftfahrzeuge,” no. September, 2019.

[78] “Products | magniX.” [Online]. Available: https://www.magnix.aero/products. [Accessed: 24-May-2021].

[79] R. W. Dyson, R. H. Jansen, N. Glenn, K. P. Duffy, and P. J. Passe, “High Efficiency Megawatt Machine Rotating Cryocooler Conceptual Design,” 2019.

[80] M. T. Fard, M. Abarzadeh, K. A. Noghanr, J. He, and K. Al-Haddad, “Si/SiC hybrid 5-level active NPC inverter for electric aircraft propulsion drive applications,” *Chinese J. Electr. Eng.*, vol. 6, no. 4, pp. 63–76, 2020.

[81] A. Deshpande, Y. Chen, B. Narayanasamy, Z. Yuan, and F. Luo, “Modular three-level t-type power electronics building block for aircraft electric-propulsion drives,” *AIAA Propuls. Energy 2020 Forum*, pp. 1–8, 2020.

[82] F. Majić, G. Efraimsson, and C. J. O’Reilly, “Potential improvement of aerodynamic performance by morphing the nacelle inlet,” *Aerosp. Sci. Technol.*, vol. 54, no. April, pp. 122–131, 2016.

[83] S. Biser *et al.*, “Design space exploration study and optimization of a distributed turbo-electric propulsion system for a regional passenger aircraft,” *AIAA Propuls. Energy 2020 Forum*, pp. 1–27, 2020.

[84] D. Meeker, “FEMM.”

[85] Ansys, “MotorCAD.” 2021.

[86] A. A. Woodworth, E. E. Shin, and M. Lizcano, “High Voltage Insulation for Electrified Aircraft,” pp. 1–11, 2020.